tion from nature and began incorporating cyclic ether features inherent to bioactive natural products.[68] We developed a series of molecular scaffolds featuring conformationally constrained cyclic ether and heterocyclic structures that mimic the binding modes of peptide/amide bonds in the S2 subsite of the HIV-1 protease active site.

3.2. Development of 3S-THF and Bis-THF P2 Ligands

Although saquinavir is a potent PI, its oral bioavailability is poor, possibly because of the presence of multiple amide/peptide bonds. Based upon the X-ray structure of saquinavir-bound HIV-1 protease, we attempted to replace two amide carbonyls (P2/P3) with cyclic ether and sulfone templates. Particularly, we planned to position the ether or sulfone such that the oxygen atom could form interactions with the protease similar to those seen for the P2 and P3 amide/peptide carbonyl functions of saquinavir. We were interested in cyclic ether features because numerous bioactive natural products contain such structural subunits, and natural products such as monensin and ginkolide do not suffer from the absorption problems inherent to peptidelike drugs.[87,88] As shown in Figure 4, replacement of the P2-asparagine of saquinavir with 3*R*-tetrahydrofuranyl glycine resulted in the very potent PI **3** (enzyme $IC_{50} = 0.05$ nM; antiviral $CIC_{95} = 8$ nM). The *R* configuration appeared to be critical to its potency.[89] We then removed the P3-quinaldic ligand and designed the corresponding stereochemically defined urethane derivative **4** ($IC_{50} = 160$ nM; concentration for 95% inhibition in cell culture (CIC_{95}) = 800 nM).[90] This lead structure was quite important as the molecular weight of **4** (515 Da) was much less than that of saquinavir (670 Da).

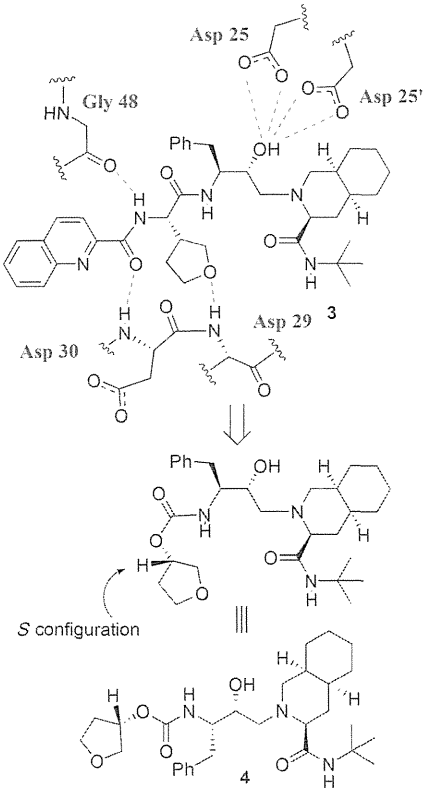

Figure 4. Inhibitors containing a cyclic ether as a P2 ligand.

The 3*S*-THF urethane **4** was significantly more potent (more than 18-fold) than the corresponding *N*-Boc derivative. Incorporation of this functionality in the hydroxyethylene-derived inhibitor **5** resulted in a marked enhancement of enzyme inhibitory and antiviral activity over that of the corresponding *N*-Boc derivative.[90] The cyclopentyl derivative **6** (Figure 5) was significantly less active even though this

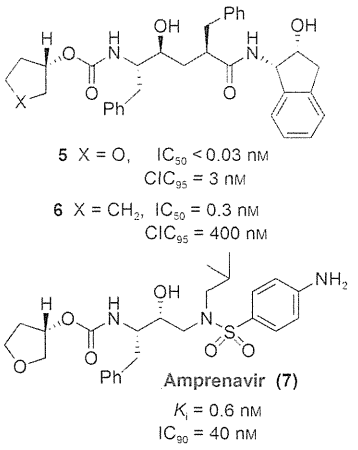

Figure 5. Potent PIs based on 3*S*-THF-urethane.

PI presumably fills the substrate binding site in the same fashion as inhibitor **5**. This result indicated that the cyclic ether oxygen is very important. A preliminary X-ray structure of **4**-bound HIV-1 protease showed that the THF-ring oxygen is involved in a weak hydrogen-bonding interaction with the NH groups of Asp29 and Asp30.[90] Introduction of this 3*S*-THF urethane in the hydroxyethylamine sulfonamide isostere developed by Vasquez et al.[91] and Tung et al.[92] resulted in PI **7** (Figure 5, VX-478).[93] This was subsequently developed into the FDA-approved inhibitor amprenavir/fosamprenavir. The X-ray structure of **7**-bound HIV-1 protease indicated that the ring fills the S2 subsite and the ring oxygen is involved in a weak interaction with the Asp29 and Asp30 backbone amides (distances of 3.4 and 3.5 Å, respectively).[93]

Based upon our preliminary development of 3*S*-THF urethane as a possible substitute for both the P2 and the P3 ligands of saquinavir, we became interested in further enhancing the binding-site interactions in the S2 subsite. This objective ultimately led us to design the stereochemically defined bicyclic (3*R*,3a*S*,6a*R*) tetrahydrofuran (bis-THF) ligand shown in Figure 6.[94] Inhibitor **8** with the (3*R*,3a*S*,6a*R*) bis-THF ligand was significantly more potent than inhibitor **9** containing the (3*S*,3a*R*,6a*S*) bis-THF ligand. Inhibitor **8** was also considerably more potent than inhibitor **4** with 3*S*-THF as the P2 ligand. Our X-ray crystallographic studies revealed that the bis-THF oxygens form effective hydrogen bonds with the backbone NH groups of Asp29 and Asp30.[94] Furthermore, the X-ray structure showed that the bicyclic ring in **8** fills the hydrophobic pocket in the S2 site more effectively than the monocycle in inhibitor **4**. Interest-

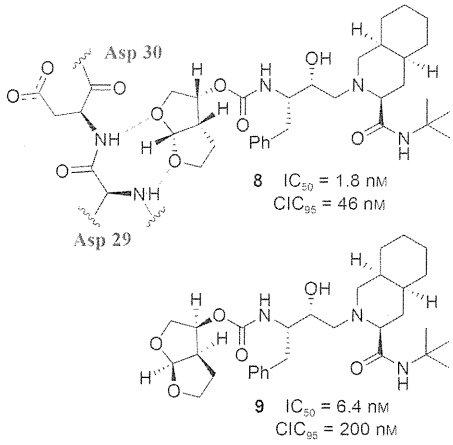

Figure 6. Design of PIs containing a bis-THF ligand.

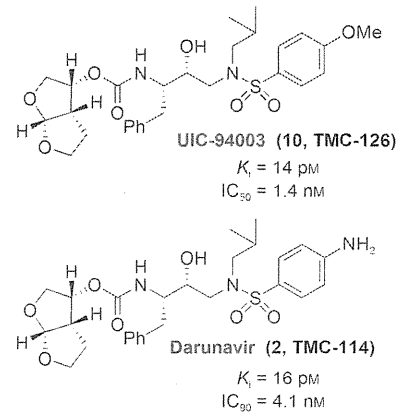

Figure 7. Potent bis-THF PIs, TMC-126 and darunavir.

ingly, however, inhibitor **8** does not form any hydrogen bonds with the protein backbone in the S2′ site.[86,94] As stated earlier, to combat drug resistance, the main emphasis of our backbone-binding strategy is to maximize ligand binding site interactions, especially to promote hydrogen-bond formation with the backbone atoms from the S2 to S2′ subsites of the protease.[50]

3.3. Design of TMC-126 and Its Relevance to the Backbone-Binding Concept

Following the design of the high-affinity and nonpeptidic bis-THF ligand, our next objective was to design an inhibitor that could form robust hydrogen bonds throughout the S2 to S2′ subsites.[50] We investigated the effect of a P2 bis-THF ligand with a number of different isosteres, including (*R*)-(hydroxyethyl)sulfonamide isosteres[91,92] with a *p*-methoxysulfonamide as the P2′ ligand.[50,81] Our initial choice of *p*-methoxysulfonamide was based upon the presumption that the methoxy oxygen would form effective hydrogen bonds with the Asp29′ and Asp30′ backbone NH groups in the S2′ subsite. As shown in Figure 7, inhibitor **10** (UIC-PI or UIC94003 and later TMC-126) exhibited marked enzyme inhibitory potency (K_i = 14 pM) and antiviral activity (ID_{50} = 1.4 nM) in CEM cell lines.[82] To obtain molecular insight into the ligand binding site interactions, a high-resolution X-ray structure of **10**-bound HIV-1 protease was determined.[95] As shown in Figure 8, both oxygen atoms of the P2 bis-THF ligand form strong hydrogen bonds with the backbone NH groups of Asp29 and Asp30 in the S2 subsite. In the S2′ subsite, the *p*-methoxy oxygen also forms strong hydrogen bonds with the backbone NH group of Asp30′ as well as with carboxylate of the Asp30′ side chain.[95] The inhibitory potency of **10** against numerous mutant HIV proteases was determined. As shown in Table 1, this inhibitor maintained very impressive potency (K_i < 100 pM) and the K_{imut}/K_{iwt} ratios were no greater than 5. This indicated that proteases with multiple mutations, which were shown to be highly resistant to approved first-generation PIs, displayed a low level of resistance against **10**.[96]

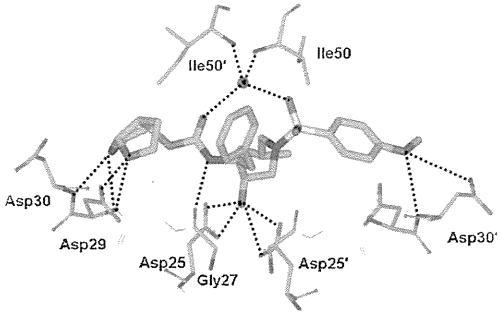

Figure 8. X-ray crystal structure of **10**-bound HIV-1 protease.

Table 1: Enzyme inhibitory potency of **10** against wild-type and mutant proteases.

Enzyme	K_i [pM]	K_{imut}/K_{iwt}	Vitality
wild type	14	1	1
D30N	< 5	0.33	0.3
V32I	8	0.57	0.5
I84V	40	2.85	1
V32I/I84V	70	5	0.7
M46F/V82A	< 5	0.33	0.1
G48V/L90M	< 5	0.33	0.1
V82F/I84V	7	0.5	0.1
V82T/I84V	22	1.57	0.1
V32I/K45I/F53L/A71V/I84V/L89M	31	2.2	0.1
V32I/L33F/K45I/F53L/A71V/I84V	46	3.3	0.1
20R/36I/54V/71V/82T	31	2.2	0.1

Inhibitor **10** also maintained excellent potency against a wide spectrum of drug-resistant HIV-1 variants with IC_{50} values ranging from 0.3 to 0.5 nM.[82] As shown in Table 2, a detailed drug-sensitivity evaluation with **10** demonstrated significant advantages compared to structurally related amprenavir and other approved PIs in terms of the emergence of drug resistance. Interestingly, viral acquisition of resistance to **10** was substantially delayed. Furthermore, **10**-resistant HIV remained sensitive to all approved PIs except amprenavir. Notably, inhibitor **10** retained impressive potency (IC_{50} = 0.5 to 5.5 nM) against multi-PI-resistant HIV-1 strains isolated from patients who were harboring drug-resistant HIV-1.[82]

Table 2: Sensitivities of **10** (TMC-126) against HIV-1 isolated from individuals having previous extensive PI treatment.

Virus[a]	IC_{50} [μM] (fold change)					
	RTV	IDV	SQV	NFV	APV	**10** (TMC-126)
wild type	0.044 (1)	0.013 (1)	0.010 (1)	0.023 (1)	0.025 (1)	0.0007 (1)
1	>1 (>23)	>1 (>77)	0.27 (27)	>1 (>43)	0.27 (11)	0.004 (6)
2	>1 (>23)	0.49 (38)	0.037 (4)	0.33 (14)	0.28 (11)	0.0013 (2)
3	>1 (>23)	0.49 (38)	0.036 (4)	>1 (>43)	0.26 (10)	0.001 (1)
4	>1 (>23)	0.21 (16)	0.033 (3)	0.09 (4)	0.31 (12)	0.0016 (2)
5	>1 (>23)	>1 (>77)	0.31 (31)	0.41 (18)	0.67 (27)	0.0024 (3)
6	>1 (>23)	0.30 (23)	0.19 (19)	>1 (>43)	0.16 (6)	0.0005 (1)
7	>1 (>23)	>1 (>77)	0.12 (12)	>1 (>43)	0.49 (20)	0.0055 (8)
8	>1 (>23)	0.55 (42)	0.042 (4)	>1 (>43)	0.15 (6)	0.001 (1)

[a] Amino acid substitutions identified in the protease-encoding regions of viruses compared to the consensus sequence cited from the Los Alamos database. See reference [82] for details.

We speculated that the impressive activity of **10** against a wide spectrum of drug-resistant HIV variants is because of its robust binding properties in the active site, particularly its extensive interactions with the backbone NH groups of aspartates in the S2 to S2′ subsites.[50] Thus, the backbone-binding strategy promoting extensive hydrogen bonds throughout the active site (S2 to S2′ subsites) may be an intriguing conceptual framework for the design of a new generation of PIs to combat drug resistance.

4. Backbone-Binding Strategy Leading to the Clinical Development of Darunavir to Combat Drug Resistance

4.1. Structural Optimization Leading to Darunavir

Based upon the results of inhibitor **10** (TMC-126), we then explored the combination of the bis-THF ligand and (*R*)-(hydroxyethyl)sulfonamide isosteres with a variety of P2′ sulfonamide functionalities. These ligands were chosen to interact with the backbone atoms in the S2′ site. These efforts led to the design and synthesis of a number of exceptionally potent PIs. However, only inhibitor **2** (Figure 7, later named TMC-114 and then darunavir) exhibited improved pharmacological properties and drug-resistance profiles.[81,97–99] We attributed the unique binding profile of **10** (UIC-94003 or TMC-126) and **2** (UIC-94017 or TMC-114) as the main contributing factor for the antiviral profile which led us to establish the design concept of protein-backbone binding as a promising strategy to overcome drug resistance.[50,100] The following section takes a closer look at the binding of darunavir and its unique antiviral profile.

4.2. Darunavir's Extensive Interactions with the Protease Backbone

Darunavir's enhanced binding affinity ($K_i = 16$ pM) is likely related to its ability to form an extensive network of hydrogen-bonding interactions within the HIV-1 protease active site. A high-resolution X-ray crystal structure of darunavir-bound HIV-1 protease revealed a number of key interactions between darunavir and the protease's backbone atoms.[69] As shown in Figure 9, the bis-THF P2 ligand forms strong hydrogen bonds with the backbone amide NH groups of Asp29 and Asp30, which anchor darunavir to the S2 subsite. On the opposite end, darunavir's *p*-aminosulfonamide interacts with the amide of Asp30′ and the carboxylic acid side chain of Asp30′ thereby stabilizing darunavir within the active site. The hydroxy group of the (hydroxyethyl)sulfonamide isostere serves as a transition-state mimic forming hydrogen bonds to the catalytic residues Asp25 and Asp25′. In addition, the urethane NH group interacts with the Gly27 carbonyl, while a tetracoordinated water molecule forms hydrogen bonds between flap residues Ile50 and Ile50′ and the urethane carbonyl and sulfonamide oxygen of darunavir. The P1′ isobutyl and P1 benzyl groups of darunavir further enhance binding through hydrophobic interactions.[69] These multiple binding interactions allow darunavir to act as a "molecular crab" tightly clutching the protein backbone.

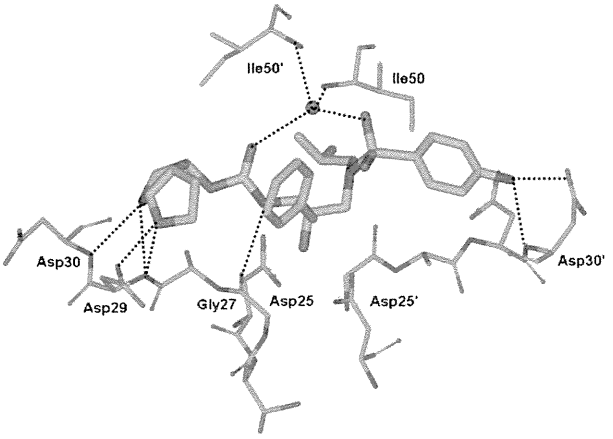

Figure 9. Darunavir binding to HIV-1 protease like a "molecular crab" (PDB code 2IEN).[69]

Unlike many first-generation PIs, the binding of darunavir to HIV-1 protease is unique. For example, while the binding of many PIs is driven by entropic gain, the binding of darunavir is highly enthalpically favored, possibly because of its numerous hydrogen-bonding interactions.[101] Another noticeable difference lies in the kinetics of darunavir's binding to the protease which shows a high association rate and very

slow dissociation rate, much lower than that of other PIs.[102] Together, these attributes provide darunavir with a specific, high-affinity binding profile and an exceptional ability to accommodate protease mutations.[103]

A final distinguishing characteristic of darunavir is that it is capable of binding to the protease at a second location, as indicated by a recent X-ray analysis.[69] The second binding site lies on the surface of the protease on one of its flexible flaps. Allosteric binding at this location may contribute to darunavir's exceptional antiviral activity by further inhibiting the function of the HIV-1 protease. Further studies examined the kinetics of darunavir binding and suggested a mixed-type competitive–uncompetitive inhibition model in contrast to first-generation PIs which exhibit strictly competitive inhibition.[104] These results were consistent with a second binding site for darunavir and likely contribute to darunavir's heightened antiviral activity profile.

4.3. Darunavir's Robust Potency against Multidrug-Resistant HIV-1 Variants

Darunavir has demonstrated remarkable antiviral potency across a broad range of HIV-1 viral strains. As depicted in Table 3, against a panel of HIV-1 isolates, darunavir outperformed many other approved PIs at inhibiting viral replication and infectivity (IC_{50} = 3–6 nM).[105] Darunavir's potent antiviral activity combined with its relatively low cytotoxicity provides it with an elevated selectivity index (> 20000 CC_{50}/EC_{50}).[105] More importantly, darunavir has consistently retained its impressive antiviral activity against a host of viral strains with resistance-related mutations. Notably, darunavir exerted very impressive activity against highly multi-PI-resistant clinical HIV-1 variants isolated from patients with AIDS who did not respond to existing antiviral regimens (results are shown in Table 4). Darunavir (**2**) exhibited excellent antiviral activity with IC_{50} values ranging from 3 to 30 nM while APV, IDV, NFV, and RTV, were virtually ineffective in blocking the replication of all multi-PI-resistant strains.[105]

Also, when surveyed against a panel of laboratory HIV-1 strains with selected resistance against other PIs, darunavir maintained excellent activity (Table 5). Only APV-resistant viral strains displayed cross-resistance to darunavir; this can be explained by the fact that APV contains a sulfonamide isostere similar to that in darunavir.[105] More elaborate studies utilizing a broad range of clinical isolates (1500+) further confirmed darunavir's remarkable properties. Darunavir maintained an EC_{50} of less than 10 nM against 75% of the variants and showed less than a tenfold change in EC_{50} compared to the wild-type against 90% of the strains.[106] In contrast, APV, SQV, IDV, RTV, NFV, and LPV displayed ED_{50} values below 10 nM against less than 30% of the viral strains and showed significantly higher levels of variability in the EC_{50} values as compared to the wild-type.[106]

A major challenge in the treatment of HIV remains the rapid emergence of drug resistance which reduces the effectiveness of antiviral treatments. The most prominent attribute of darunavir that sets it apart from other PIs is its high genetic barrier to the development of viral resistance. Early attempts to select for darunavir-resistant HIV viruses in vitro proved difficult; resistance developed very slowly after

Table 3: Sensitivities of **2** and selected anti-HIV agents against HIV-$1_{Ba\text{-}L}$, HIV-2_{ROD}, and HIV-2_{EHO}.

Virus	Cell type	Mean IC_{50} [nM][a] SQV	RTV	IDV	NFV	APV	AZT	DRV (**2**)
HIV-$1_{Ba\text{-}L}$	PBMC	18	39	25	17	26	9	3
HIV-2_{ROD}	MT-2	3	130	14	19	230	18	3
HIV-2_{EHO}	MT-2	6	240	11	29	170	11	6

[a] All assays were conducted in duplicate or triplicate; the data represent mean IC_{50} values from three independent experiments. IC_{50} were evaluated with PHA-PBMC and the inhibition of p24 Gag protein production by the drug as an end point. MT-2 cells were exposed to the virus and cultured, and IC_{50} values were determined by MTT assay. See references [82] and [105] for details.

Table 4: Activity of inhibitor **2** against HIV-1 clinical isolates in PHA-PBMCs.

Virus[a]	IC_{50} values [μM] SQV	APV	IDV	NFV	RTV	DRV (**2**)
HIV-$1_{ERS104pre}$ (wt X4)	0.010	0.023	0.018	0.019	0.027	0.003
HIV-1_{MOKW} (wt R5)	0.004	0.011	0.018	0.033	0.032	0.003
HIV-1_{TM} (MDR X4)	0.23 (23)	0.39	>1 (>56)	0.54 (28)	>1 (>37)	0.004 (1)
HIV-1_{MM} (MDR R5)	0.30 (30)	0.34	>1 (>56)	>1 (>53)	>1 (>37)	0.02 (7)
HIV-1_{JSL} (MDR R5)	0.35 (35)	0.75 (33)	>1 (>56)	>1 (>53)	>1 (>37)	0.029 (10)
HIV-1_{A} (MDR X4)	0.14 (14)	0.16 (7)	>1 (>56)	0.36 (19)	>1 (>37)	0.004 (1)
HIV-1_{B} (MDR X4)	0.31 (31)	0.34 (15)	>1 (>56)	>1 (>53)	>1 (>37)	0.013 (4)
HIV-1_{C} (MDR X4)	0.037 (4)	0.28 (12)	>1 (>56)	0.44 (23)	>1 (>37)	0.003 (1)
HIV-1_{G} (MDR X4)	0.029 (3)	0.25 (11)	0.39 (22)	0.32 (17)	0.44 (16)	0.004 (1)

[a] Amino acid substitutions identified in the protease-encoding regions of viruses compared to the consensus sequence cited from the Los Alamos database. See reference [105] for details.

Table 5: Activity of DRV against PI-resistant HIV-1 laboratory strains.

Virus	Amino acid substitution	EC_{50} [μM][a]					
		SQV	RTV	IDV	NFV	APV	DRV
$HIV\text{-}1_{NL4\text{-}3}$	wild type	0.009	0.018	0.011	0.020	0.027	0.003
$HIV\text{-}1_{SQV5\mu M}$	L10I, G48V, I54V, L90M	>1 (>111)	>1 (>56)	>1 (>91)	0.30 (15)	0.17 (6)	0.005 (2)
$HIV\text{-}1_{RTV5\mu M}$	M46I, V82F, I84V	0.013 (1)	>1 (>56)	0.31 (28)	0.24 (12)	0.61 (23)	0.025 (8)
$HIV\text{-}1_{IDV5\mu M}$	L10F, L24I, M46I, L63P, A71V, G73S, V82T	0.015 (2)	>1 (>56)	>1 (>91)	0.74 (37)	0.33 (12)	0.029 (10)
$HIV\text{-}1_{NFV5\mu M}$	L10F, D30N, K45I, A71V, T74S	0.031 (3)	0.09 (5)	0.28 (25)	>1 (>50)	0.093 (3)	0.003 (1)
$HIV\text{-}1_{APV5\mu M}$	L10F, V32I, M46I, I54M, A71V, I84V	0.020 (2)	>1 (>56)	0.31 (28)	0.21 (11)	>1 (>37)	0.22 (73)

[a] MT-4 cells were exposed to each HIV-1 strain ($100\times TCID_{50}$), and the inhibition of p24 Gag protein production by the drug was used as an end point. Numbers in parentheses represent the fold changes of the IC_{50} values for each isolate relative to that of $HIV\text{-}1_{NL4\text{-}3}$. See reference [105].

multiple passages and only at concentrations of less than 200 nM of darunavir (Figure 10).[106] Later studies showed that although the wild-type HIV virus did not propagate darunavir resistance easily, HIV-1 isolates from antiretroviral-experienced patients were capable of acquiring resistance-related mutations.[107] During the POWER clinical trials, 11 amino acid substitutions were correlated to darunavir resistance including V11I, V32I, L33F, I47V, I50V, I54L/M, G73S, L76V, I84V, and L89V, of which I50V, I54M/L, L76V, and I84V are considered the major mutations.[108,109] A28S was later identified as an amino acid substitution distinctly associated with darunavir and not caused by other PIs.[110] By itself, A28S results in a significant reduction in enzyme fitness which can be restored in part by the secondary mutation I50V. Darunavir resistance to A28S is believed to occur from a shift in position of the P2 sulfonamide that alters its ability to hydrogen bond with the protease causing a decrease in binding affinity.

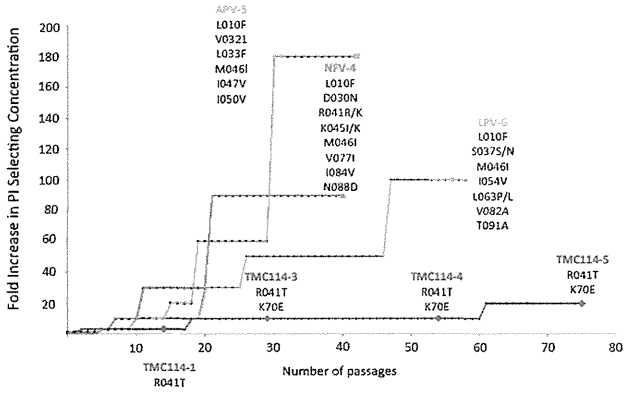

Figure 10. In vitro selection of resistant HIV strains in the presence of NFV, APV, LPV, and TMC-114(DRV). The figure is modified from Figure 4 in reference [106].

4.4. Darunavir Inhibits Dimerization of HIV-1 Protease

Darunavir's impressive antiviral profile can be attributed in part to its small flexible conformation and its ability to form extensive hydrogen-bonding interactions with the protease backbone, which imparts a high binding affinity. Another contributing factor is darunavir's unique ability to act as a dual inhibitor, blocking not only the cleavage of the natural peptide substrate but also inhibiting dimerization of the HIV-1 protease. An active HIV-1 protease consists of two chains of 99 amino acids each that combine or dimerize into a single catalytically active quaternary structure. Dimerization of the monomer subunits is essential for activity and thus its inhibition represents a distinct mechanism for inhibiting viral replication.[111] Darunavir blocks this dimerization process at concentrations as low as 0.01 μM.[112] Further investigation is currently ongoing. TPV is the only other PI besides darunavir that has been shown to possess this property.[112] While capable of blocking the dimerization of individual monomers, neither darunavir nor TPV is able to cause disassociation of an assembled protease unit.

5. Retaining Backbone Binding and Designing Exceptionally Potent Bis-THF-Derived PIs

5.1. The Effect of Benzodioxolane Sulfonamide at the S2′ Site

We continued to explore structural modifications that would form additional hydrogen bonds with the protease backbone residues leading to inhibitors with higher affinity. We have incorporated a benzodioxolane sulfonamide as the P2′ ligand and this has provided inhibitor **11** (GRL-98065) shown in Figure 11. This turned out to be an exceedingly potent inhibitor with significant antiviral activity ($K_i = 11$ pM and $IC_{50} = 1.1$ nM).[113] As can be seen in Table 6, inhibitor **11** was evaluated against a wide spectrum of multidrug-resistant clinical isolates and inhibitor **11** outperformed other approved PIs including darunavir. It maintained significant antiviral activity (6–12-fold change) similar to darunavir. Furthermore, **11** was evaluated against PI-resistant HIV-1 variants and was found to have a unique antiviral activity profile (Table 7). Against the PI-resistant variants, cross-resistance to APV was observed. Interestingly, SQV and ATV remained active against viral strains selected against **11** which contain the A28S mutation. This was linked to TMC-126 resistance and resulted in a significant loss in fitness of the protease.[113]

We determined the crystal structure of **11**-bound HIV-1 protease at 1.6 Å resolution. This structure has provided important molecular insight into the inhibitor potency and

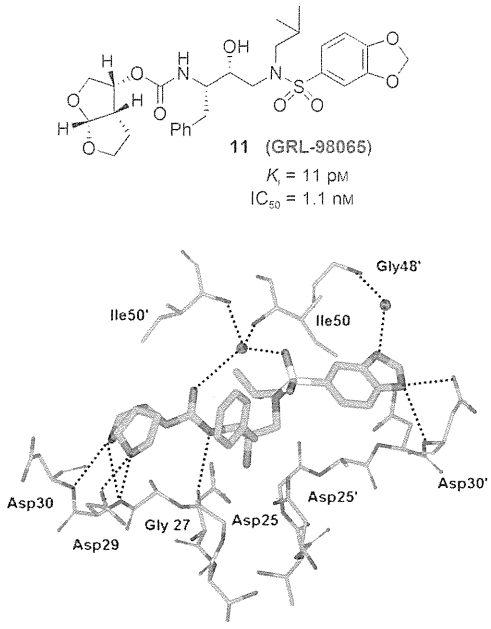

Figure 11. Structure of **11** and the X-ray crystal structure of **11**-bound HIV-1 protease.

drug-resistance profile.[113] Structural analyses revealed that **11** is involved in extensive interactions with the backbone atoms of the amino acids in the protease active site (Asp29 and Asp30, Figure 11) in the S2 to S2′ subsites. These interactions are important for its potency and wide-spectrum activity against multi-PI-resistant HIV-1 variants. Moreover, these interactions are maintained in crystal structures of **11**-bound drug-resistant mutants.[114] Comparison of the crystal structure of **11** with the crystal structure of darunavir (Figure 9) showed that the interactions with the S2 site are similar, but the nature of the hydrogen bonds with residues differs in the S2′ region. A water-mediated interaction of one of the benzodioxolane oxygens with flap residue Gly48′ is not observed for darunavir (**2**). These differences in interactions may account for the improvement of IC_{50} values of **11** compared to those of darunavir.[113]

5.2. Design and Clinical Development of Bis-THF PIs with Novel P1 Functionalities

Numerous potent PIs have been designed based upon the privileged bis-THF ligand.[67,84] As shown in Figure 12, brecanavir (**12;** BCV/GW0385), which was developed by GlaxoSmithKline, contains a bis-THF P2 ligand, a benzodioxolane P2′ ligand, and a substituted P1 ligand.[115,116] It showed femtomolar enzyme inhibitory potency (K_i = 15 fM) and subnanomolar antiviral activity with an IC_{50} value of 0.7 nM (wild-type virus). Also, BCV exhibited IC_{50} values of 1.1 nM and 4.8 nM against two MDR viral strains, EP13 HIV-1 and D545701 HIV-1, respectively.[115] BCV exhibited sub- to

Table 6: Antiviral activities of GRL-98065 (**11**) against multidrug-resistant clinical isolates.

Virus[a]	EC_{50} [nM][b]					
	SQV	RTV	NFV	APV	DRV	**11** (GRL-98065)
HIV-$1_{ERS104pre}$ (wild-type X4)	8	25	15	29	3.8	0.5
HIV-$1_{MDR/TM}$ (X4)	180 (23)	>1000 (>40)	>1000 (>67)	300 (10)	4.3 (1)	3.2 (6)
HIV-$1_{MDR/MM}$ (R5)	140 (18)	>1000 (>40)	>1000 (>67)	480 (17)	16 (4)	3.8 (8)
HIV-$1_{MDR/JSL}$ (R5)	290 (36)	>1000 (>40)	>1000 (>67)	430 (15)	27 (7)	6 (12)
HIV-$1_{MDR/B}$ (X4)	270 (34)	>1000 (>40)	>1000 (>67)	360 (12)	40 (11)	3.9 (8)
HIV-$1_{MDR/C}$ (X4)	35 (4)	>1000 (>40)	420 (28)	250 (9)	9 (2)	2.7 (5)
HIV-$1_{MDR/G}$ (X4)	33 (4)	>1000 (>40)	370 (25)	320 (11)	7 (2)	3.4 (7)

[a] The amino acid substitutions identified in the protease-encoding region compared to the consensus type B sequence cited from the Los Alamos database. See reference [113] for details. [b] Effective concentration by 50%.

Table 7: Antiviral activities of **11** against laboratory PI-resistant HIV-1 variants.

Virus	EC_{50} [μM] of drug[a]								
	SQV	RTV	IDV	NFV	APV	LPV	ATV	DRV	**11** (GRL-98065)
HIV-1_{NL4-3}	0.007	0.033	0.034	0.033	0.026	0.031	0.0042	0.0030	0.0003
HIV-$1_{SQV5\mu M}$	>1 (>143)	>1 (>30)	>1 (>29)	0.48 (15)	0.33 (13)	0.27 (9)	0.326 (78)	0.0058 (2)	0.006 (20)
HIV-$1_{RTV5\mu M}$	0.010 (1)	>1 (>30)	0.25 (7)	0.21 (6)	0.28 (11)	0.16 (5)	0.018 (4)	0.018 (6)	0.0025 (8)
HIV-$1_{IDV5\mu M}$	0.059 (8)	>1 (>30)	>1 (>29)	0.47 (14)	0.17 (7)	0.26 (8)	0.06 (14)	0.015 (5)	0.0037 (12)
HIV-$1_{NFV5\mu M}$	0.024 (3)	0.051 (2)	0.27 (8)	>1 (>30)	0.060 (2)	0.024 (1)	0.021 (5)	0.0033 (1)	0.0024 (8)
HIV-$1_{APV5\mu M}$	0.031 (4)	0.29 (9)	0.200 (6)	0.27 (8)	>1 (>38)	0.23 (7)	0.003 (1)	0.33 (110)	0.032 (107)
HIV-$1_{LPV1\mu M}$	0.032 (5)	>1 (>30)	>1 (>29)	0.49 (15)	0.31 (12)	0.31 (10)	0.040 (10)	n.d.	0.0075 (25)
HIV-$1_{ATV1\mu M}$	0.037 (5)	0.12 (4)	0.388 (11)	0.22 (7)	0.20 (8)	0.033 (1)	0.33 (79)	0.0034 (1)	0.0015 (5)
HIV-$1_{GRL98065p40}$	0.032 (5)	0.38 (12)	0.28 (8)	0.34 (10)	>1 (>38)	0.19 (6)	0.011 (3)	0.21 (70)	0.18 (600)

[a] MT-4 cells were exposed to 100 $TCID_{50}$ (dose for 50% infection in cell culture) of each HIV-1, and inhibition of p24 Gag protein production by each drug was used as an end point. Numbers in parentheses represent *n*-fold changes in the EC_{50} values for each isolate compared to the EC_{50} values for wild-type HIV-1_{NL4-3}. All assays were conducted in duplicate or triplicate, and data shown are derived from the results of three independent experiments. n.d. = not determined. See reference [113] for details.

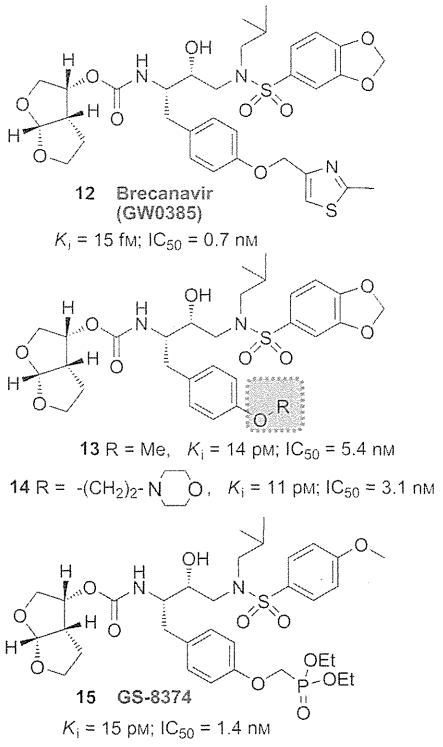

Figure 12. Structures of PIs **12–15.**

low nanomolar IC_{50} values with low cross-resistance against a panel of 10 highly resistant and specifically PI-resistant HIV-1 isolates.[115] Furthermore, BCV was tested against a panel of 55 clinical isolates from PI-experienced patients and it maintained low nanomolar IC_{50} values (0.1–14.9 nM) for all isolates. The majority of isolates (80%) displayed IC_{50} values at or below 0.8 nM.[117,118] This inhibitor had undergone clinical development at the phase III level. However, brecanavir's clinical trials were terminated because of formulation issues.[119]

We have investigated structure-based modifications of the P1 side chain of inhibitor **11**. Of particular interest, we attempted to incorporate a basic amine or a cyclic ether functionality to improve aqueous solubility and other pharmacological properties. Both PIs **13** and **14** have shown very potent antiviral activity.[120]

Inhibitor **15** (GS-8374) containing a P2 bis-THF unit, a P2′ *p*-methoxybenzesulfonamide ligand, and a diethylphosphonylmethoxy group attached to the P1 phenyl ligand was developed by researchers at Gilead Sciences.[121] The phosphonate functionality was designed to promote better intracellular retention without interfering with the protease binding site of **10** (TMC-126). This PI (**15**) displayed an excellent resistance profile.[121,122] It exhibited a mean 6.2-fold change in EC_{50} values (range 0.6–26 nM) from the wild-type HIV. Inhibitor **15** displayed a mean 29.8-fold change (1.0–157 nM) and 23.6-fold change of EC_{50} values (1.2–121 nM) compared to darunavir and BCV, respectively. Towards a possible explanation of this marked resistance suppression, it was proposed that the phosphonate moiety acted as an anchor point in the solvent medium and enhanced the degeneracy of the binding state of the inhibitor by providing favorable entropic compensation following protease mutations. Interestingly, selection of HIV-1 strains exposed to **15** did not exhibit any signs of RAM (resistance-associated mutation) even after six months.[123] GS-8374 has been reported to show more favorable pharmacological and metabolic profiles than other PIs. In the X-ray crystal structure of **15**-bound HIV-1 protease the binding profiles for the P2 bis-THF and the P2′ methoxysulfonamide ligands are similar to those observed in the X-ray structure of the **10**-bound HIV-1 protease. A comparison of the two structures showed that one of the phosphonate ethyl moieties of **15** is bound in a hydrophobic cleft on the surface of protease.[121] GS-8374 with a *p*-diethylphosphonate at the P1 phenyl residue exhibited a better resistance profile than to BCV, which contains a substituted methylthiazole at P1.[123]

5.3. The Effect of a C4-Methoxy Bis-THF Ligand at the S2 Site

The HIV-1 protease flaps are flexible in the apoenzyme form, but they are closed when inhibitors bind and show minimal change in their backbone conformation.[53,124] As can be seen in Figure 11, a novel water-mediated interaction with Gly48′ through the benzodioxolane oxygen may be responsible for its superb antiviral and drug-resistance profile. Based upon the X-ray structure of **10**-bound HIV-1 protease, we envisioned that heteroatom-containing substituents at the C4 position of the bis-THF ligand would be ideally positioned to interact with the backbone NH group of Gly48.[95] Therefore, we synthesized a series of new PIs incorporating C4-alkoxy-substituted bis-THF ligands.[125] As shown in Figure 13, inhibitor **16** with a 4*R*-methoxy group has better enzyme inhibitory potency (K_i = 2.9 pM) than inhibitor **10** (K_i = 14 pM). The 4*R* isomer **16** was 12-fold more potent than the corresponding 4*S* isomer **17**. Larger alkyl groups at C4, such as benzyloxy substituents, led to significant reduction in potency. An X-ray structure of **16**-bound HIV-1 protease (Figure 13) showed extensive interactions of the inhibitor with the protease active site similar to those of inhibitor **10**.[125] However, it appears that the oxygen of the 4*R*-methoxy group forms a unique water-mediated hydrogen bond with the NH group of Gly48. The improvement in binding affinity of **16** may be due to this water-mediated hydrogen bond with the backbone NH group of Gly48.[125]

5.4. Design of Macrocyclic Inhibitors with a Bis-THF Unit at the S2 Site

In an effort to fill the hydrophobic pocket in the S1′–S2′ subsites with flexible macrocycles, we investigated bis-THF-derived macrocyclic inhibitors involving P1′–P2′ ligands that can retain all major hydrogen-bonding interactions with the protein backbone similar to those of inhibitor **10** and darunavir but effectively fill the hydrophobic pocket in the S1′ and S2′ subsites.[95] The design perception for these macrocycles evolved from the observation that certain mutations lead to decreased van der Waals interactions and an increase in size of the hydrophobic pocket in the S1′

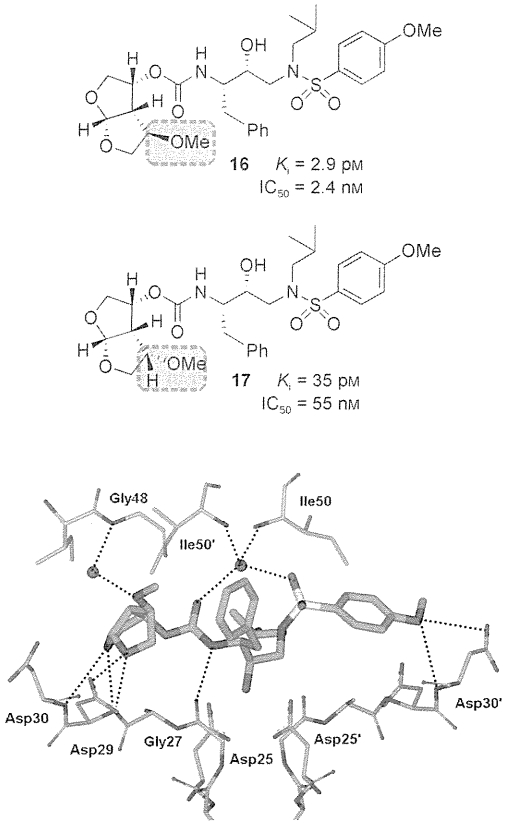

Figure 13. Structures of PIs **16** and **17** and the X-ray structure of **16**-bound HIV-1 protease.

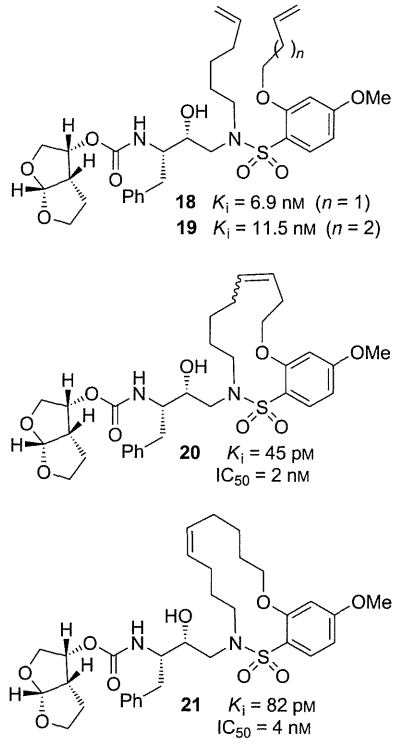

Figure 14. Structures of acyclic and macrocyclic PIs **18**–**21**.

subsite. The structural studies of A-77003[126] indicated that the V82A mutant results in decreased van der Waals interactions with the phenyl rings in both the S1 and S1′ subsites.[127] Also, there was evidence of the repacking of the inhibitor side chain and protease atoms in the S1 subsite. Based upon this insight, we envisioned that 11- to 15-membered saturated and unsaturated macrocycles would effectively fill the S1′–S2′ subsites. As shown in Figure 14, macrocyclic inhibitors **20** and **21** displayed excellent enzyme inhibitory and antiviral activity; however, their acyclic homologues were significantly less potent. Also, saturated inhibitors were less active than their unsaturated analogues.[95]

To ascertain if the structural effects led to improved drug-resistance properties, inhibitors **20** and **21** were evaluated against a panel of clinical wild-type X_4-HIV-1 isolates (HIV-$1_{ERS104pre}$) along with various multidrug-resistant clinical X_4- and R_5-HIV-1 isolates using PBMCs as target cells.[95,105] As shown in Table 8, the potency of both inhibitors against HIV-$1_{ERS104pre}$ (IC_{50} = 7 and 5 nM, respectively) was superior to that of the approved inhibitors IDV, APV, and LPV but nearly twofold less potent than darunavir (IC_{50} = 3 nM).[95] Inhibitor **20** showed better potency than amprenavir against HIV-$1M_{DR/C}$, HIV-$1M_{DR/G}$, HIV-$1M_{DR/TM}$, and HIV-$1M_{DR/JSL}$ and was six times more potent against HIV-$1M_{DR/MM}$. Inhibitor **21** also displayed superior potency against HIV-$1M_{DR/C}$ and HIV-$1M_{DR/G}$ (greater than 12- and 15-fold, respectively) compared to amprenavir.[95,128] Furthermore, both macrocyclic PIs prevented the replication of HIV-1_{NL4-3} variants selected against up to 5 μM of saquinavir, lopinavir, and indinavir with IC_{50} values of 20 nM to 46 nM. We have determined an X-ray crystal structure of **20**-bound HIV-1 protease at 1.17 Å resolution. As can be seen in Figure 15, both P2 and P2′ ligands are involved in extensive hydrogen-

Table 8: Antiviral activity of macrocyclic inhibitors against multidrug-resistant clinical isolates in PHA-PBMCs.

Virus[a]	IC_{50} value [μM]						
	SQV	IDV	APV	LPV	DRV	**21**	**20**
HIV-$1_{ERS104pre}$ (WT X4)	0.008	0.043	0.030	0.034	0.003	0.007	0.005
HIV-$1_{MDR/B}$ (X4)	0.27 (34)	>1 (>23)	>1 (>33)	>1 (>29)	0.019 (6)	0.089 (13)	0.037 (7)
HIV-$1_{MDR/C}$ (X4)	0.032 (11)	>1 (>23)	0.37 (12)	>1 (>29)	0.008 (3)	0.029 (4)	0.044 (9)
HIV-$1_{MDR/G}$ (X4)	0.030 (4)	0.34 (5)	0.43 (14)	0.26 (8)	0.023 (5)	0.028 (4)	0.057 (11)
HIV-$1_{MDR/TM}$ (X4)	0.26 (33)	>1 (>23)	0.32 (11)	>1 (>29)	0.004 (1)	0.072 (10)	0.027 (6)
HIV-$1_{MDR/MM}$ (R5)	0.19 (24)	>1 (>23)	0.21 (7)	>1 (>29)	0.011 (4)	0.055 (8)	0.033 (7)
HIV-$1_{MDR/JSL}$ (R5)	0.30 (37)	>1 (>23)	0.62 (21)	>1 (>29)	0.027 (9)	0.21 (30)	0.073 (15)

[a] The amino acid substitutions identified in the protease-encoding region compared to the consensus type B sequence cited from the Los Alamos database. See reference [95] for details.

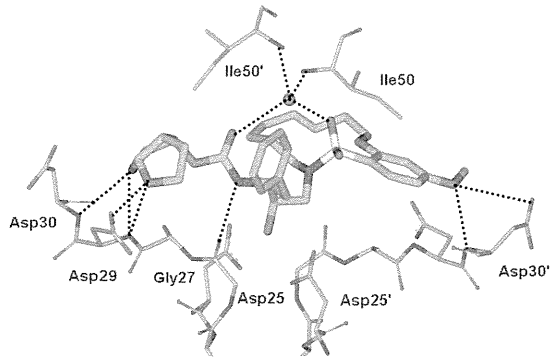

Figure 15. X-ray structure of HIV-1 protease bound to the macrocyclic inhibitor **20**. All strong hydrogen-bonding interactions are shown as dotted lines.

bonding interactions with the protein backbone atoms in both the S2 and S2′ subsites, similar to inhibitor **10**. The crown-shaped P1′–P2′macrocycle nicely fills the S1′ pocket. Interestingly, the macrocycle acts more or less like a spring and pushes against the P1 phenyl ring. This causes a rotation about 30° towards Asp29′ along the backbone which is absent in the X-ray structure of **10**-bound HIV-1 protease. Both macrocyclic PIs were able to maintain excellent potency against multidrug-resistant clinical isolates possibly because of their ability to make extensive hydrogen bonds with the protease backbone as well as their hydrophobic interactions in the S1′–S2′ subsites.[95]

6. Probing the Backbone-Binding Concept as a Design Strategy to Combat Drug Resistance

6.1. Development of Cyclopentanyltetrahydrofuran (Cp-THF) as a Novel P2 Ligand

To further investigate the merit of targeting the protein backbone as a design strategy, based upon various protein–ligand X-ray structures, we decided to design structurally different cyclic-ether-derived ligands that were not related to bis-THF ligand. This effort led to the design of a stereochemically defined bicyclic hexahydrocyclopentanofuran (Cp-THF) as the P2 ligand. Incorporation of this ligand in the hydroxyethylaminosulfonamide isostere provided a series of exceptionally potent PIs.[51] We positioned the cyclic ether oxygen in the Cp-THF ring to form hydrogen bonds with the backbone NH groups of Asp29 and Asp30. As can be seen in Figure 16, replacing the bis-THF in darunavir with a new Cp-THF ligand provided inhibitor **22**, which exhibited sub-nanomolar enzyme inhibitory potency nearly ten times less than that of darunavir ($K_i = 16$ pM). We believed that binding of the Cp-THF ligand in the S2 subsite was distinct from the bis-THF ligand and may have caused a slight shift in position of the remainder of the inhibitor structure within the active site.[51] We then speculated that modifications of the P2′ aniline could allow improved interactions with the NH groups of Asp29′ and Asp30′ in the S2′ subsite. As shown, we have incorporated a hydroxymethylsulfonamide as the P2′ ligand

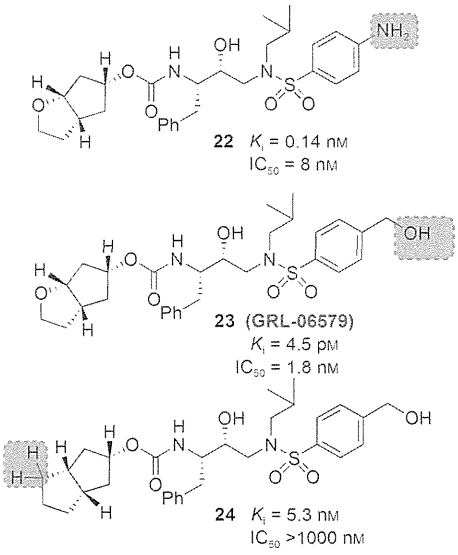

Figure 16. Structures of Cp-THF-related PIs.

and the resulting inhibitor **23** showed a 30-fold improvement of enzyme inhibition ($K_i = 4.5$ pM) compared to **22**. In addition, it has shown very impressive antiviral potency ($IC_{50} = 1.8$ nM) similar to that of inhibitor **10**. In order to probe the importance of the Cp-THF ring oxygen, we synthesized inhibitor **24** in which the oxygen is replaced with a methylene group. Interestingly, **24** displayed a more than 1100-fold loss of enzyme inhibitory potency compared to **23**. Furthermore, **24** exhibited a drastic loss in antiviral activity ($IC_{50} > 1000$ nM). This result indicated that the Cp-THF ring oxygen is involved in critical interactions in the active site.

We determined the X-ray crystal structure of **23**-bound HIV-1 protease at a 1.35 Å resolution and this high-resolution structure provided critical molecular insight into the interactions at the ligand binding site.[51] As shown in Figure 17, inhibitor **23** makes extensive interactions in the active site similar to darunavir. The P2′ hydroxy group forms a strong hydrogen bond to the backbone NH group of Asp30′and a water-mediated contact with the side chain oxygen of Asp30′. The ring oxygen of the P2 Cp-THF ligand forms a strong hydrogen bond with the backbone NH group of Asp29 and a weak hydrogen bond with Asp30. These interactions cannot

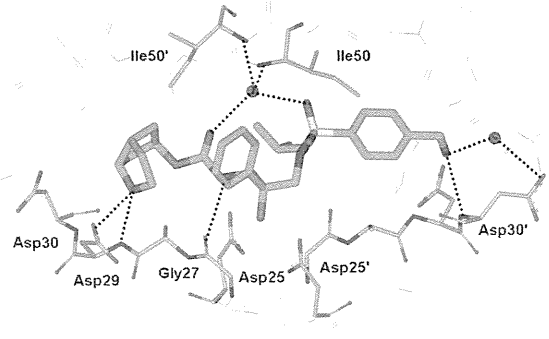

Figure 17. X-ray structure of **23**-bound HIV-1 protease.

occur for inhibitor **24** which lacks the ring oxygen and this may explain why **24** is significantly less potent than **23**. This result illustrates the importance of forming hydrogen bonds with the protease backbone in the S2 subsite and suggests that simply filling the binding space of this site is not sufficient to induce tight binding and elicit a biological response.

We superimposed the X-ray structure of **23**-bound HIV-1 protease (wild-type) with the three most highly mutated drug-resistant proteases.[51] These structures showed minimal root-mean-square deviation of the α-carbon backbone atoms (0.5 to 1.1 Å) suggesting inhibitor **23** should retain good to excellent contacts with the backbone of the mutant proteases. As it turned out, inhibitor **23** exerted very potent activity against HIV-1 isolates (HIV-1_{LAI} and HIV-$1_{Ba\text{-}L}$) in both MT-2 cells and PHA-PBMC (Table 10). Furthermore, as evident in Table 9, inhibitor **23** retained significant antiviral activity against a panel of HIV-1 drug-resistant viral strains. Inhibitor **23** displayed the most potent activity ($IC_{50} = 3$ nM) against HIV-1 clinical strain HIV-1_{ET}, which had been isolated from a drug-naive patient. Furthermore, six drug-resistant clinical strains containing 10–12 amino acid substitutions associated with protease inhibitor resistance (HIV-1_B, HIV-1_C, HIV-1_G, HIV-1_{TM}, HIV-1_{EV}, and HIV-1_{ES}) were isolated from patients with HIV-1 infection having received 7–11 different antiviral agents for 24 to 81 months.[82,105] All tested approved PIs were highly resistant. However, inhibitor **23** exerted highly potent activity against all of these six variants with IC_{50} values ranging from 4 nM to 52 nM. Inhibitor **23** was also highly potent against HIV-1_K with an IC_{50} value as low as 3 nM. This data indicate that inhibitor **23** is highly active against a wide spectrum of drug-resistant variants.[51]

Table 10: Antiviral activity (IC_{50}) of **23** in PBMC and MT-2 cells.

Virus	IC_{50} [nM][a]					
	SQV	RTV	INV	NFV	APV	**23**
HIV-1_{LAI}	14	43	32	14	34	1.8
HIV-$1_{Ba\text{-}L}$	18	36	24	7	29	2.0
HIV-1_{LAI}	24	34	26	10	24	1.8
HIV-2_{EHO}	1.9	290	13	20	440	21

[a] Data represent the mean value of three determinations. See reference [51] for details.

6.2. Design of meso-Hexahydrocyclopenta-1,3-dioxolane as a P2 Ligand

As we have seen, the oxygen atom in the Cp-THF ring of **23** is critical to its superb antiviral and anti-drug-resistance properties. Based upon the X-ray structure of **23**-bound HIV-1 protease, we then speculated that a corresponding *meso*-hexahydrocyclopenta-1,3-dioxolane ligand would be able to maintain interactions similar to those of the Cp-THF ligand. Essentially, we would insert an oxygen atom into the Cp-THF ring and form a *meso*-hexahydrocyclopenta-1,3-dioxolane ligand which would greatly reduce the stereochemical complexity and allow for a simplified synthetic pathway. In addition to the synthetic advantage, we postulated that the additional ether oxygen may engage in hydrogen-bonding interactions with the protease thereby enhancing the potency of the PIs. Figure 18 depicts the structure and potency of a number of PIs incorporating a *meso* ligand.[129]

The *syn* isomer **25** demonstrated enzyme inhibitory potency and antiviral activity comparable to that of the Cp-THF-derived PI **23**, whereas the *anti* isomer **27** showed a threefold decrease in potency. Unlike the results with the Cp-THF ligand, incorporation of a hydroxymethyl group in the P2′ ligand resulted in a slight reduction in potency. We next explored a 1,4-dioxane P2 ligand; the resulting inhibitor **28** exhibited a significant reduction in antiviral potency. A larger trioxepane system also provided a less active PI. We evaluated **25** against a panel of multidrug-resistant HIV-1 variants, and the results are shown in Table 11. Inhibitor **25** exhibited antiviral activity comparable to that of the approved PIs SQV and APV, while it outperformed IDV. However, **25** was not as active as darunavir against the wild-type or drug-resistant HIV-1 clinical variants. We determined an X-ray structure of **28**-bound HIV-1 protease at 1.07 Å resolution (Figure 19). The inhibitor binds with extensive interactions in the protease active site. Interestingly, one of the dioxane oxygens forms a hydrogen bond with the backbone NH group of Asp29. The other oxygen is involved in a water-mediated hydrogen bond with the amide NH group of Gly48. These interactions with Gly48 were similar to those reported for several peptide substrate analogues.[15,64] How-

Table 9: Antiviral activity of **23** against a panel of HIV-1 viral strains.

Virus	IC_{50} [nM] values						
	SQV	RTV	IDV	NFV	APV	DRV	**23**
HIV-1_{ET}	17	15	30	32	23	n.d.	3
HIV-1_B	230	>1000	>1000	>1000	290	10.2	15
HIV-1_C	100	>1000	500	310	300	3.5	5
HIV-1_G	59	>1000	500	170	310	3.7	20
HIV-1_{TM}	250	>1000	>1000	>1000	220	3.5	4
HIV-1_{EV}	>1000	>1000	>1000	>1000	>1000	n.d.	52
HIV-1_{ES}	>1000	>1000	>1000	>1000	>1000	n.d.	31
HIV-1_K	20	58	260	>1000	68	3	3

[a] Amino acid substitutions identified in the protease-encoding region of HIV-1_B (B), HIV-1_C (C), HIV-1_G (G), HIV-1_{TM} (TM), HIV-1_{EV} (EV), HIV-1_{ES} (ES), HIV-1_{ET} (ET), HIV-1_K (NFV_R) as compared to the consensus B sequence cited from the Los Alamos data base. All values were determined in triplicate. The IC_{50} values were determined by employing PHA-PBMC as target cells and the inhibition of p24 Gag protein production as the endpoint. See reference reference [51] for details.

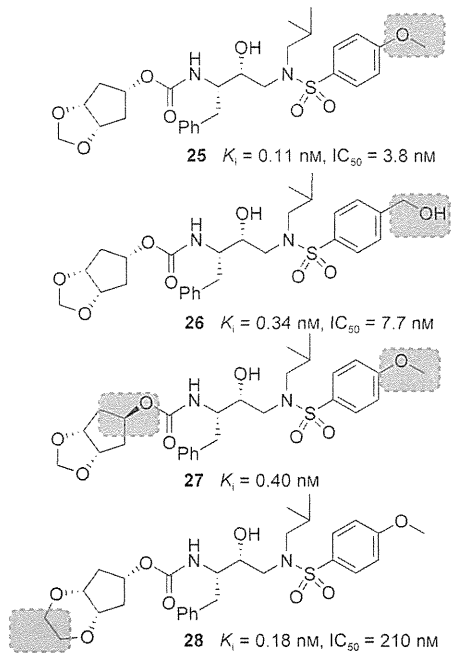

Figure 18. Enzyme K_i values and antiviral potency of PIs **25–28**.

ever, this interaction with Gly48 has not been previously utilized in ligand design. Based upon this X-ray structure, we created an active model of **25**. It appears that smaller the 1,3-dioxolane forms an additional hydrogen bond with the backbone NH group of Asp30.[129] This additional hydrogen bond may explain the increased antiviral activity of **25** relative to **28**.

6.3. Alkoxy/Hydroxy-Cp-THF Ligands and Their Effect on Drug-Resistance Properties

As described above, the *meso*-dioxolane-derived inhibitor exhibited very potent enzyme inhibitory and antiviral activity.[129] As shown in Figure 19, we speculated that both oxygens of the dioxolane ring in **25** form hydrogen bonds with backbone Asp29 and Asp30 NH groups and also form a water-mediated hydrogen bond with the Gly48 backbone NH group. Based upon these possible interactions in the ligand binding site, we subsequently designed a 3-hydroxy-Cp-THF derivative to interact with the Gly48 NH group in the flap.[130] We synthesized a stereochemically defined alkoxy-Cp-THF

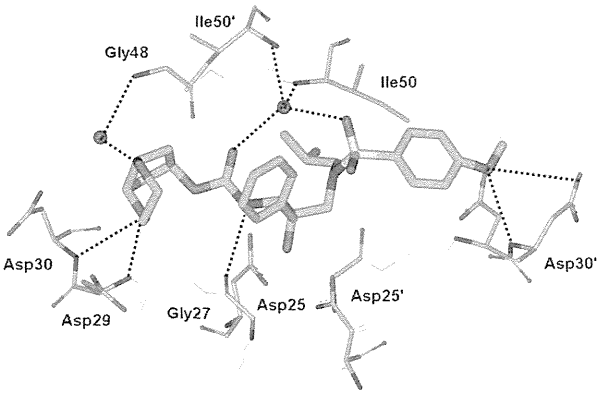

Figure 19. X-ray structure of inhibitor **28** bound to the active site of wild-type HIV-1 protease.

derivative and converted it into the PIs shown in Figure 20. As can be seen, inhibitor **30** with a 3*R*-hydroxy group showed the most potent antiviral activity comparable to that of

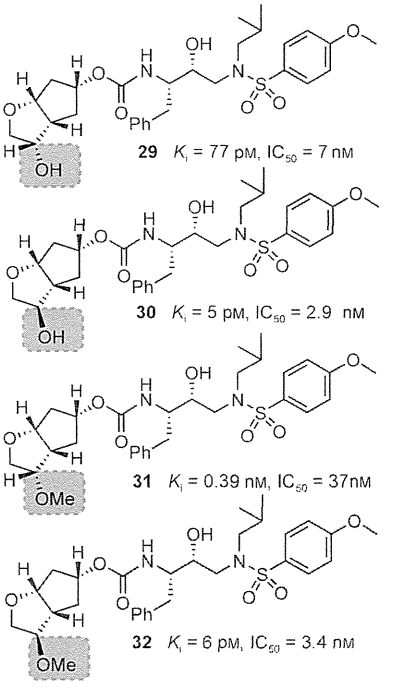

Figure 20. Structures of PIs **29–32** with alkoxy/hydroxy-Cp-THF ligands.

Table 11: Antiviral activity of inhibitor **25** against clinical HIV-1 isolates in PBMC cells.

Virus[a]	IC_{50} values [nM]				
	SQV	IDV	APV	DRV	**25**
$HIV\text{-}1_{ERS104pre}$ (wild-type: X4)	12	26	33	3.5	29
$HIV\text{-}1_{MDR/MM}$ (R5)	190 (16)	>1000 (>38)	300 (9)	17 (5)	150 (5)
$HIV\text{-}1_{MDR/JSL}$ (R5)	330 (28)	>1000 (>38)	430 (13)	26 (7)	550 (19)
$HIV\text{-}1_{MDR/C}$ (X4)	36 (3)	>1000 (>38)	230 (7)	7 (2)	300 (10)
$HIV\text{-}1_{MDR/G}$ (X4)	29 (2)	290 (11)	340 (10)	7 (2)	340 (12)
$HIV\text{-}1_{MDR/A}$ (X4)	81 (7)	>1000 (>38)	100 (3)	3 (1)	21 (1)

[a] Amino acid substitutions identified in the protease-encoding region compared to the consensus type B sequence cited from the Los Alamos database, see reference [129] for details.

darunavir. The related inhibitor **29** with a 3*S*-hydroxy group was also quite potent. We prepared the corresponding 3-methoxy-Cp-THF ligands and the resulting inhibitors **31** and **32** showed stereochemical preferences and potencies similar to those of the corresponding hydroxy derivatives.[130]

We then determined the X-ray crystal structure of **30**-bound HIV-1 protease at 1.23 Å resolution. As shown in Figure 21, the Cp-THF ring oxygen forms a strong hydrogen bond with the Asp29 NH group and a rather weak hydrogen bond with the Asp29 carboxylate. The 3-hydroxy group appears to form a nice water-mediated hydrogen bond with the Gly48 backbone NH group.

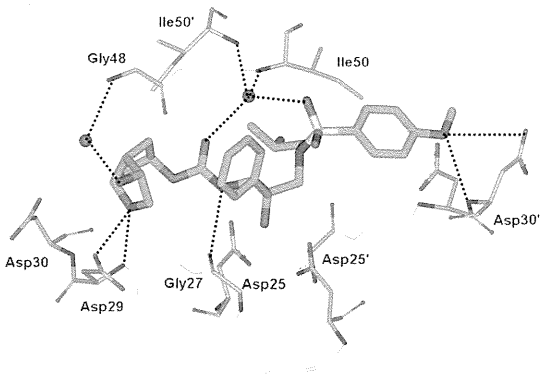

Figure 21. X-ray structure of **30**-bound HIV-1 protease.

PIs **29** and **30** were evaluated against a panel of multidrug-resistant HIV-1 variants and compared with the approved PIs darunavir and APV (Table 12). The activity of inhibitor **30** against various multidrug-resistant HIV-1 variants is similar

Table 12: Comparison of the antiviral activity of **29**, **30**, and of other PIs against multidrug-resistant HIV-1 variants.

Virus[a]	IC_{50} [μM] (fold change)			
	APV	DRV	**29**	**30**
$HIV\text{-}1_{ERS104pre}$ (wild type)	0.030	0.0037	0.020	0.0029
$HIV\text{-}1_{MDR/B}$	0.93 (31)	0.036 (10)	>1 (>50)	0.029 (10)
$HIV\text{-}1_{MDR/C}$	0.26 (9)	0.013 (4)	>1 (>50)	0.022 (7)
$HIV\text{-}1_{MDR/G}$	0.38 (12)	0.0023 (1)	0.27 (13)	0.0045 (2)
$HIV\text{-}1_{MDR/TM}$	0.19 (6)	0.0019 (1)	0.041 (2)	0.0031 (1)

[a] Amino acid substitutions identified in the protease-encoding region compared to the consensus type B sequence cited from the Los Alamos database, see reference [130] for details.

to that of darunavir.[130] The changes in the IC_{50} values with **30** were similar to those with darunavir. In contrast, PI **29** with a 3*S*-hydroxy ligand lost potency significantly. Also, APV showed high IC_{50} values and lower resilience against the drug-resistant HIV-1 strains examined. The X-ray structure of **30**-bound HIV-1 protease and its resistance profile further supported the backbone-binding strategy for combating drug resistance.

6.4. Further Enhancing the Backbone Interactions of Cp-THF-Derived PIs at the S1′ Site and Probing the Effect on Drug-Resistance Properties

In addition to ligand design to enhance interactions with the protein backbone in the S2 subsite, we have also expanded our design concept in other regions of the protease active site. We particularly planned to design PIs with new P1′ ligands in place of the isobutyl group of **23** that could interact with backbone atoms as well as fill the hydrophobic pocket in S1′ subsite. We explored the incorporation of stereochemically defined 2-pyrrolidinone and oxazolidinone functionalities so that the pyrrolidinone NH group could form a hydrogen bond with Gly27′ and its carbonyl group could interact with Arg8′ in the S1′ site.[131] Our initial plan was to examine the potential of the new P1′ ligand in combination with Cp-THF and bis-THF ligands. We also wanted to address the question of whether enhancement of backbone-binding interactions would lead to PIs with improved drug-resistance profiles. The results of this investigation are summarized in Figure 22. Inhibitor **33** with (*S*)-methyl-2-pyrrolidinone as the P1′ ligand

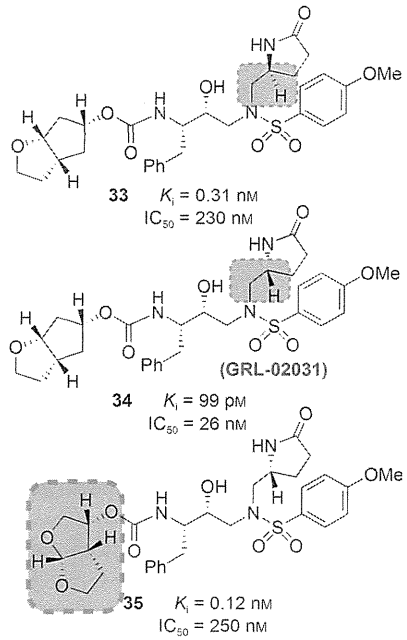

Figure 22. Structures and potency of PIs **33–35.**

showed good enzyme inhibitory potency but its antiviral IC_{50} value was 230 nM. The (*R*)-methyl-2-pyrrolidinone derivative **34** showed improvement in both the K_i value and antiviral activity (IC_{50} = 26 nM) relative to *S*-pyrrolidine derivative **33**. For the combination of bis-THF as P2 and (*R*)-methyl-2-oxazolidinone as P1′ ligands, however, the antiviral activity was significantly less than that of **10**. The antiviral potency of **34** was nearly ten times less than that of **23**. This is possibly a result of the poor cellular permeability of the polar 2-oxazolidinone functionality. Nevertheless, inhibitor **34** is a very potent inhibitor with antiviral activity comparable to that of FDA-approved PIs such as IDV, APV and LPV.[131]

To obtain molecular insight into various ligand binding site interactions, we determined a high-resolution X-ray crystal structure of **34**-bound HIV-1 protease at 1.29 Å resolution.[131] As shown in Figure 23 the interactions between the inhibitor and the active site are quite extensive. Most strikingly, the P1′-pyrrolidinone exists in two conformations. In one conformation, the pyrrolidinone NH group is engaged in a hydrogen bond with the Gly27′ carbonyl and the pyrrolidinone carbonyl forms a water-mediated hydrogen bond with the Arg8′ side chain. In another conformation, the pyrrolidinone ligand fills the hydrophobic pocket and the carbonyl group makes a weak hydrogen bond with the Val82′ backbone NH group. Other binding interactions of the Cp-THF ligand in the S2 site are similar to those of **23** and the methoxy oxygen in S2′ forms a strong hydrogen bond with the backbone NH group of Asp30′ and the side-chain carboxylate group.[131]

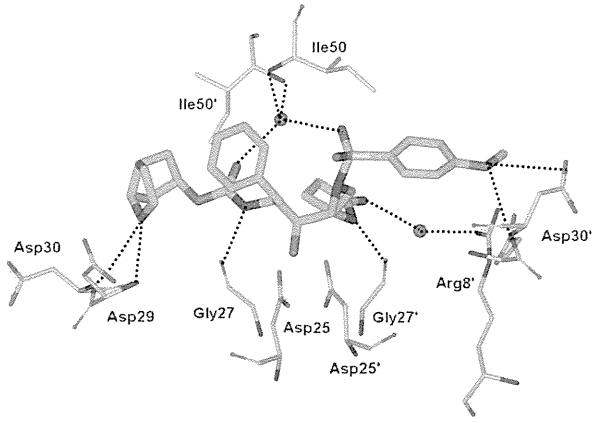

Figure 23. X-ray structure of **34**-bound HIV-1 protease.

Inhibitor **34** was evaluated against a wide spectrum of laboratory and clinical wild-type and multidrug-resistant HIV-1 strains. Table 13 shows its anti-HIV activity against selected clinical isolates highly resistant to multiple PIs.[131,132] As can be seen, inhibitor **34** was highly potent against various clinical isolates tested. Except darunavir, all other approved PIs failed to exert comparable activity. However, inhibitor **34**, like darunavir, potently inhibited all seven primary strains. Particularly, **34** maintained nearly full potency except with the R5 phenotype where it lost potency slightly (by less than twofold). Overall, the interactions of inhibitor **34** (GRL-02031) with backbone atoms particularly in the S1′ subsite were enhanced compared to those with inhibitor **23**. These polar interactions and the conformational flexibility of the P1′ oxazolidinone most likely contributed to its robust activity against multidrug-resistant HIV-1 variants.[132]

7. Conformationally Flexible P2 Ligands Capable of Forming Extensive Interactions with the Backbone

7.1. Design of Flexible Cyclic Polyethers as P2 Ligands and Their Effect on Drug-Resistance Properties

Following exploration of our PIs based on *meso* P2 ligands, we continued to examine ways in which we could reduce the stereochemical complexity of the bis-THF ligand while maintaining key backbone interactions and accommodating variations in the amino acid side chains within the active site occurring after viral mutations. To probe this, we turned to cyclic-polyether-derived P2 ligand systems possessing flexible rings capable of repacking within the binding pocket in response to mutational changes.[133] Based on this proposition, we removed the shared C–C bond from bis-THF producing the flexible eight-membered-ring inhibitor **36** shown in Figure 24. Unfortunately, **36** displayed significantly

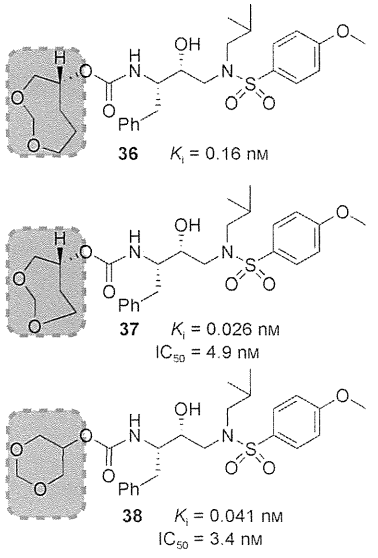

Figure 24. Structures and potency of PIs containing cyclic polyethers.

Table 13: Anti-HIV activity of **34** against selected clinical isolates highly resistant to multiple protease inhibitors.

Virus[a]	Phenotype	EC_{50} [μM]				
		IDV	APV	LPV	DRV	GRL-02031 (**34**)
HIV-$1_{ERS104pre}$ (wild-type)	X4	0.028	0.025	0.03	0.0036	0.028
HIV-1_{TM} (MDR)	X4	>1 (>36)	0.25 (10)	0.73 (24)	0.0036 (1)	0.029 (1)
HIV-1_{MM} (MDR)	R5	>1 (>36)	0.32 (13)	0.72 (24)	0.019 (5)	0.042 (2)
HIV-1_{C} (MDR)	X4	>1 (>36)	0.35 (14)	0.32 (11)	0.015 (4)	0.023 (1)
HIV-1_{G} (MDR)	X4	0.29 (10)	0.33 (13)	0.14 (5)	0.014 (4)	0.027 (1)

[a] Amino acid substitutions identified in the protease-encoding regions of HIV-$1_{ERS104pre}$, HIV-1_{TM}, HIV-1_{MM}, HIV-1_{C}, and HIV-1_{G} compared to the consensus B sequence cited from the Los Alamos database, see references [131] and [132].

lower enzyme inhibitory potency than darunavir. Reducing the ring size to a seven-membered ring restored enzyme inhibitory activity, and a preference for the *R* stereoisomer was revealed as the corresponding PI with epimeric P2 ligand displayed significant loss in potency ($K_i = 0.16$ nM, $IC_{50} =$ 30 nM). Further reductions in ring size led to the six-membered-ring inhibitor **38** which was also highly potent. In general, expanding the ring to larger polycyclic ethers (ten-membered rings and larger) resulted in a drastic loss in potency. The ether oxygens within these ring systems are critical for maintaining high levels of enzyme inhibition activity. The removal of either oxygen from **37** resulted in a significant loss in activity.

An X-ray crystal structure of **37**-bound HIV-1 protease was determined at 1.00 Å resolution. The majority of binding interactions within the active site are similar in nature to those with inhibitor **10** (TMC-126) except for interactions in the S2 site. As shown in Figure 25, one of the oxygens of the 1,3-dioxepane ligand is involved in hydrogen bonding with Asp29 and Asp30 NH groups. The other oxygen is involved in a unique interaction with the Gly48 NH group through a water molecule.[133]

Both PIs **37** and **38** were further evaluated for their antiviral activity against a panel of clinically relevant HIV-1 isolates (Table 14). While they were less potent than darunavir, both compounds outperformed the approved PIs RTV and IDV and were comparable in antiviral activity to APV. These results suggested that the ability of the P2 ligand in **37** to maintain hydrogen-bonding interactions with the protein backbone may be responsible for the improved drug-resistance profiles of **37** over other PIs examined. The design of PIs using the concept of maximized backbone binding has led to PIs characterized by high potency against both wild-type and multidrug-resistant HIV-1 strains.[50]

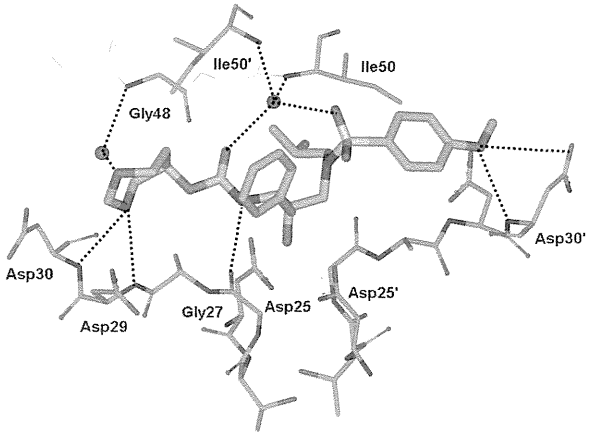

Figure 25. X-ray structure of **37**-bound HIV-1 protease.

7.2. Further Optimization of Bis-THF Ligands and the Design of a P2 TP-THF Ligand

We subsequently evaluated options to improve upon the bis-THF ligand of darunavir. An analysis of the X-ray structure of darunavir-bound HIV-1 protease (Figure 9) revealed that the bis-THF ether oxygens are involved in hydrogen-bonding interactions with the amide N-H groups of Asp29 and Asp30 at a distance of 2.9 and 3.1 Å, respectively. We conceptualized that incorporation of a larger ring system might promote closer more effective hydrogen bonding to these backbone residues and result in a more favorable alignment between the cyclic ether oxygen and the Asp30 amide N-H bond. These factors might result in stronger hydrogen bonds and higher affinity inhibitors. In addition, a larger ring size may promote favorable hydrophobic interactions within the S2 subsite and allow additional flexibility to better accommodate steric changes caused by protease mutations. Therefore, we synthesized and evaluated a series of PIs containing a tetrahydropyranyl-THF (Tp-THF) P2 ligand.[134] As shown in Figure 26, consistent with bis-THF, the bicyclic ligand in **39** (GRL-0476) with its 4*S* configuration is more effective than the epimeric ligand. Like the bis-THF ligand, both cyclic ether oxygens are critical for binding as their respective replacement with methylene groups resulted in a significant loss in potency. We have also prepared PIs **40** and **41** incorporating a *p*-methoxybenzyl side chain as the P1 ligand and *p*-methoxysulfonamide and *p*-aminophenylsulfonamide as the P2′ ligands, respectively. Our detailed drug-resistance studies of **40** and **41** showed that both PIs were very potent against multi-PI-resistant HIV-1 variants.[135]

To obtain molecular insight, we have created an active model of **39** starting from the X-ray crystal structure of **10** (TMC-126). The conformation of **39** was optimized using the

Table 14: Anti-HIV activity of **37** and **38** against selected clinical isolates highly resistant to multiple protease inhibitors.

Virus[a]	IC_{50} [nM] values					
	IDV	RTV	APV	DRV	**37**	**38**
ERS104pre (wild-type)	26	34	33	3.5	20	6
MDR/TM	>1000 (>38)	>1000 (>29)	290 (9)	4 (1)	220 (11)	64 (10)
MDR/MM	>1000 (>38)	>1000 (>29)	300 (9)	17 (5)	250 (13)	110 (5)
MDR/JSL	>1000 (>38)	>1000 (>29)	430 (13)	26 (7)	500 (25)	330 (55)
MDR/B	>1000 (>38)	>1000 (>29)	320 (10)	26 (7)	340 (17)	230 (38)
MDR/C	>1000 (>38)	>1000 (>29)	230 (7)	7 (2)	210 (11)	160 (27)
MDR/G	290 (11)	>1000 (>29)	340 (10)	7 (2)	360 (18)	300 (50)
MDR/A	>1000 (>38)	>1000 (>29)	100 (3)	3 (1)	20 (1)	13 (2)

[a] Amino acid substitutions identified in the protease-encoding region compared to the consensus type B sequence cited from the Los Alamos database, see reference [133].

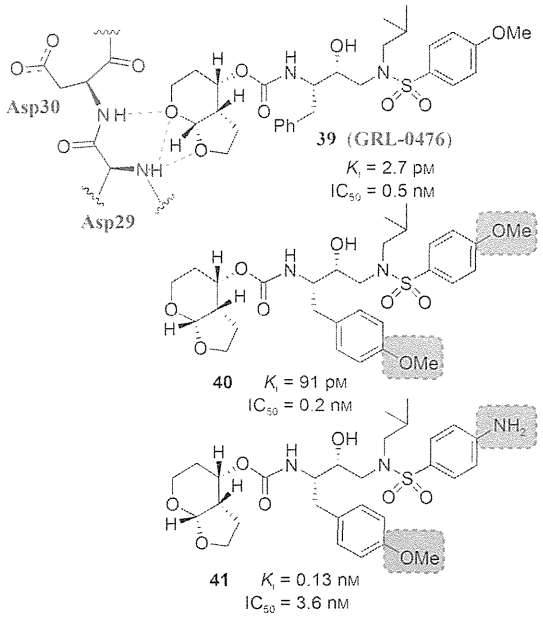

Figure 26. Structure and potency of Tp-THF-derived PIs.

MMFF94 force field.[136] It appeared that the cyclic ether oxygens of Tp-THF are within hydrogen-bonding distance to Asp29 and Asp30 backbone NH groups in the S2 subsite. Other active-site interactions are similar to those in the X-ray structure of **10**-bound HIV-1 protease.[95] As depicted in Table 15, against a panel of multidrug-resistant clinical isolates, inhibitor **39** outperformed two other approved PIs (APV and LPV) displaying a high level of antiviral activity against all the strains with EC_{50} values ranging from 2.6 to 27.5 nM. These results are comparable to those of **10** (TMC-126), and **39** is more potent than darunavir in absolute terms; however, the fold changes in efficacy factors between viral strains are similar.

8. Further Improvement of Drug Resistance by Targeting Protein Backbone and Protein–Ligand Interactions

In our efforts to target the protein backbone as a design strategy to combat drug resistance, we have developed a variety of intriguing ligands and scaffolds and generated diverse inhibitors with exceptional potency and drug-resistance profiles. Our next objective was to further optimize a ligand structure that could maintain critical backbone interactions and at the same time effectively fill the hydrophobic pocket in the active site and maximize protein–ligand interactions. Towards this objective, we elected to append functionalities to the bis-THF ligand to further improve the drug-resistance properties of the PIs. As shown in Figure 27, based upon the overlay of the X-ray structures of darunavir-bound[69] and SQV-bound[86] HIV-1 protease, we planned to

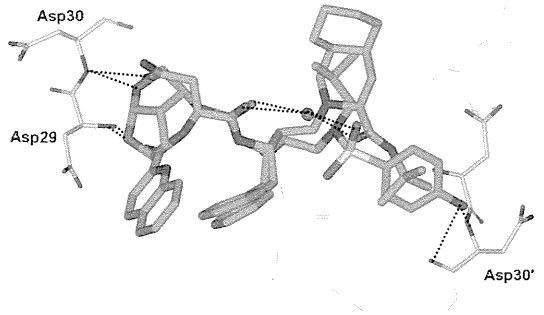

Figure 27. Overlay of the X-ray structures of darunavir-bound and SQV-bound HIV-1 protease.

fill the hydrophobic pocket occupied by the quinaldic moiety of SQV. Particularly, we have speculated that the fusion of another tetrahydrofuran ring on the bis-THF ligand would provide additional ligand binding site interactions. While such an oxatricyclic ligand could have a number of possible stereochemical motifs, including *syn-syn-syn* (*SSS*-type) and *syn-anti-syn* (*SAS*-type) isomers, our model based upon overlay structures in Figure 27 suggested that the *SAS*-type ligand-based inhibitor would make enhanced interactions in the S2 subsite. We subsequently synthesized both *SAS*- and *SSS*-oxatricyclic ligands in a stereoselective manner and prepared the respective PIs **42** and **43** shown in Figure 28.[137]

Inhibitor **42** (GRL-0519A) with the *syn-anti-syn* configuration of the tris-THF rings exhibited a tenfold better enzyme inhibitory potency over the *syn-syn-syn* derivative **43**. Inhibitor **42** also displayed better antiviral activity than **43**. An X-ray structure of **42**-bound HIV-1 protease was determined at 1.27 Å (Figure 29).[137] Analysis of this structure revealed a

Table 15: Comparison of the antiviral activity of **39** against multidrug-resistant clinical isolates.

Virus[a]	Phenotype	EC_{50} [μM]			
		ATV	LPV	DRV	**39** (GRL-0476)
$HIV\text{-}1_{ERS104pre}$ (wild type)	X4	0.0027	0.031	0.004	0.0019
$HIV\text{-}1_{MDR/B}$	X4	0.470 (174)	>1 (>32)	0.034 (9)	0.0145 (8)
$HIV\text{-}1_{MDR/C}$	X4	0.039 (14)	0.437 (14)	0.009 (2)	0.0037 (2)
$HIV\text{-}1_{MDR/G}$	X4	0.019 (7)	0.181 (6)	0.026 (7)	0.0026 (1)
$HIV\text{-}1_{MDR/TM}$	X4	0.075 (28)	0.423 (14)	0.022 (6)	0.0275 (14)
$HIV\text{-}1_{MDR/MM}$	R5	0.205 (76)	0.762 (25)	0.017 (4)	0.0050 (3)
$HIV\text{-}1_{MDR/JSL}$	R5	0.293 (109)	>1 (>32)	0.023 (6)	0.0275 (14)

[a] For details of amino acid substitutions identified in the protease-encoding region of $HIV\text{-}1_{ERS104pre}$, $HIV\text{-}1_{B}$, $HIV\text{-}1_{C}$, $HIV\text{-}1_{G}$, $HIV\text{-}1_{TM}$, $HIV\text{-}1_{MM}$, and $HIV\text{-}1_{JSL}$ and the assay protocol, see references [134] and [135].

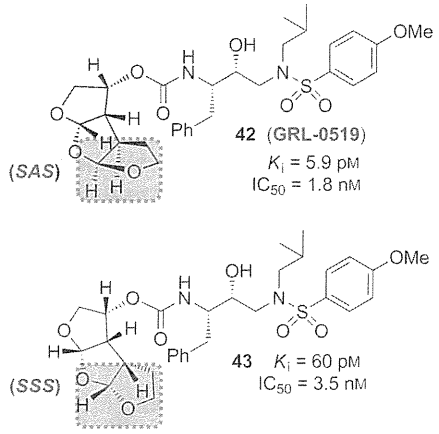

Figure 28. Structures and potency of PIs **42** and **43**.

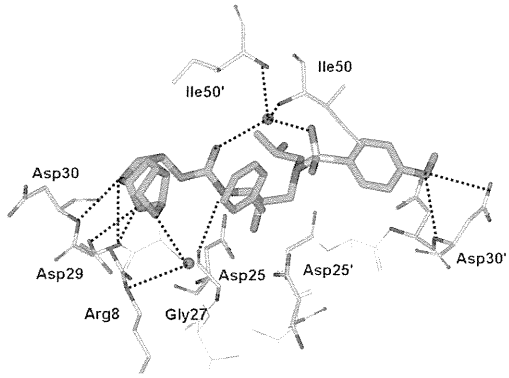

Figure 29. X-ray structure of **42**-bound HIV protease (PDB code 30K9).[137]

number of additional interactions within the S2 subsite not seen with the bis-THF unit of darunavir or TMC-126. The two top THF ring oxygens are involved in hydrogen-bonding interactions with the backbone NH groups of Asp29 and Asp30. The second THF oxygen appears to form a hydrogen bond with the carboxylate side chain of Asp29. As expected, the third THF ring fills the S2 subsite very nicely. The third THF ring also participates in a semicircular hydrogen-bonding network with three conserved water molecules that surround the guanidine side chain of Arg8.

Inhibitor **42** proved to be extremely potent against various multidrug-resistant HIV-1 variants, with IC_{50} values ranging from 0.6–4.3 nM, nearly a 10-fold improvement over the potency of darunavir (Table 16). The emergence of GRL-0519A-resistant HIV-1 in vitro was substantially delayed compared to selected approved PIs.[137] Also, very strikingly, GRL-0519A more potently blocked protease dimerization by at least a factor of 10 compared to darunavir as examined in the fluorescence resonance energy transfer based HIV-1 expression assay employing cyan and yellow fluorescent protein tagged protease monomers.[112] The present data suggested that the GRL-0519 class of PIs may be further developed as potential therapeutic agents for the treatment of primary and multidrug-resistant HIV-1 infections.

Table 16: Antiviral activity of **42**, amprenavir (APV), and darunavir (DRV) against multidrug-resistant clinical isolates in PHA-PBMCs.

Virus[a]	EC50 [μm]		
	APV	DRV	**42** (GRL-0519)
$HIV\text{-}1_{ERS104pre}$ (wild-type)	0.032	0.005	0.0006
$HIV\text{-}1_{MDR/B}$	0.521 (16)	0.028 (6)	0.0043 (7)
$HIV\text{-}1_{MDR/C}$	0.357 (11)	0.011 (2)	0.0009 (2)
$HIV\text{-}1_{MDR/G}$	0.485 (15)	0.031 (6)	0.0027 (5)
$HIV\text{-}1_{MDR/TM}$	0.488 (15)	0.031 (6)	0.0022 (4)
$HIV\text{-}1_{MDR/MM}$	0.291 (9)	0.016 (3)	0.0027 (5)
$HIV\text{-}1_{MDR/JSL}$	0.419 (13)	0.024 (5)	0.0028 (5)

[a] See reference [137] for details.

9. Summary and Outlook

Our specific interest in the chemistry and biology of natural products brought a unique perspective to our design and synthesis of HIV-1 protease inhibitors for the treatment of HIV infection and AIDS. Our initial academic pursuit was focused on addressing the question of whether we could design natural product derived ligands or templates that could mimic the biological mode of action of peptide bonds and alleviate problems inherent to peptide-based drugs. Nature has been optimizing various cyclic ether/polycyclic ether templates for millions of years in various biological micro-environments involving biosynthetic enzymes. Inspired by nature and based upon X-ray structures of protein–ligand complexes, we invoked the idea of designing stereochemically defined cyclic ether or polyether-like molecular features to replace peptide bonds and effectively fill the hydrophobic pockets in the active site of HIV-1 protease. We envisioned positioning cyclic ether oxygen to mimic the biological action of a peptide carbonyl group and the cyclic functionality would make necessary van der Waals interactions in the hydrophobic pocket. These research efforts led to the creation of a variety of conceptually novel molecular templates that are entirely nonpeptidic but interact with HIV-1 protease with remarkable affinity. Our many X-ray structural studies of inhibitor-bound HIV-1 proteases provided strong evidence that such a cyclic ether/polyether oxygen indeed serves as an effective mimic of the carbonyl of a peptide/amide functionality. Also, such cyclic units nicely fill the hydrophobic pockets in the enzyme active site.

Following the development of various nonpeptide high-affinity ligands, we turned toward addressing the issue of drug resistance. We were interested in optimizing inhibitor structures against wild-type HIV-1 protease as well as against known mutant proteases. This objective led us to examine X-ray structures of inhibitor-bound wild-type HIV-1 proteases as well as the X-ray structures of a number of mutant proteases. Superimposition of these X-ray structures evidenced only minimal distortion of the backbone conformation. This led to our proposition of targeting the protein backbone as a strategy to evade drug resistance. By maximizing hydrogen-bonding interactions with the protein backbone, we have essentially created a "molecular crab" capable of latching on and holding tightly in the enzyme active site.

Using the combination of our in-depth antiviral studies, along with drug-resistance, and X-ray crystallographic studies, we have documented the practicality and usefulness of the backbone-binding design strategy to combat drug resistance. The combination of our ligand-design efforts inspired by polyether natural products, and subsequent inhibitor design efforts targeting the protease backbone to combat drug resistance, culminated in the discovery and ultimate development of darunavir, the first FDA-approved treatment for patients with multidrug-resistant HIV-1 variants. Its indications were later generalized for all patients with HIV infection and AIDS. Furthermore, we discovered that darunavir possesses a dual mechanism of action and is a potent inhibitor of HIV-1 protease dimerization.

The discovery of darunavir marked an important turning point in the paradigm of designing HIV PIs. Our work has led us to develop the backbone-binding concept as an effective means to mitigate viral adaptability. We have continued to apply our backbone-binding design strategy resulting in the design and synthesis of a variety of exceedingly potent HIV-1 protease inhibitors with intriguing structural features. Interestingly, GRL-02031 retained near full potency against a panel of multidrug-resistant HIV-1 variants. Also, the design of GRL-0519 marked a tenfold improvement in antiviral activity over that of darunavir with retention of potency against a wide range of clinically relevant multidrug-resistant strains. The backbone-binding concept may prove useful as a guide for the design of antiretroviral agents in other areas as well. We will continue to utilize and develop this concept in our future designs as we strive to meet the challenges of today's medicine.

This work was supported by the National Institute of Health (GM53386). We thank Dr. K. V. Rao (Purdue University) for helpful discussions.

Received: April 20, 2011
Published online: January 31, 2012

[1] E. Domingo, C. K. Biebricher, M. Eigen, J. J. Holland in *Quasispecies and RNA Virus Evolution: Principles and Consequences*, Eurekah, Georgetown, **2001**, preface.
[2] M. Burnet, D. O. White in *Natural History of Infectious Disease*, Cambridge University Press, London, **1972**.
[3] J. Needham, L. Gwei-djen in *Science and Civilization in China, Vol. 6* (Ed.: N. Sivin), Cambridge University Press, Cambridge, **1999**, p. 134.
[4] A. Waterson, L. Wilkinson in *An Introduction to the History of Virology*, Cambridge University Press, Cambridge, **1978**, pp. 23–34.
[5] F. Fenner, F. M. Burnett in *Portraits of Viruses: A History of Virology* (Eds.: F. Fenner, A. Gibbs), S. Karger AG, Basel, **1988**, pp. 1–37.
[6] J. B. Brooksby in *Portraits of Viruses: A History of Virology* (Eds.: F. Fenner, A. Gibbs), S. Karger AG, Basel, **1988**, pp. 124–146.
[7] WHO, Summary of SARS Cases, http://www.who.int/csr/sars/country/country2003_08_15.pdf, **2003**.
[8] WHO, Cumulative Number of Confirmed Human Cases of Avian Influenza A/(H5N1) Reported to WHO, http://www.who.int/csr/disease/avian_influenza/country/cases_table_2011_02_02/en/index.htm, **2011**.
[9] UNAIDS Report on the global HIV/AIDS epidemic, http://www.unaids.org/en/media/unaids/contentassets/documents/unaidspublication/2010/20101123_globalreport_en.pdf, **2010**.
[10] F. Barre-Sinoussi, J. Chermann, F. Rey, M. Nugeyre, S. Chamaret, J. Gruest, C. Dauguet, C. Axler-Blin, et al., *Science* **1983**, *220*, 868–871.
[11] R. C. Gallo, P. S. Sarin, E. P. Gelmann, M. Robert-Guroff, E. Richardson, V. S. Kalyanaraman, D. Mann, G. D. Sidhu, R. E. Stahl, S. Zolla-Pazner, J. Leibowitch, M. Popovic, *Science* **1983**, *220*, 865–867.
[12] T. Lyle in *Comprehensive Medicinal Chemistry II, Vol. 7* (Eds.: J. Taylor, D. Triggle), Elsevier Science Maryland Heights, **2007**, pp. 329–371.
[13] Y. Mehellou, E. De Clercq, *J. Med. Chem.* **2010**, *53*, 521–538.
[14] L. Menéndez-Arias, *Antiviral Res.* **2010**, *85*, 210–231.
[15] C. Flexner, *Nat. Rev. Drug Discovery* **2007**, *6*, 959–966.
[16] H. Mitsuya, S. Broder, *Nature* **1987**, *325*, 773–778.
[17] N. E. Kohl, E. A. Emini, W. A. Schleif, L. J. Davis, J. C. Heimbach, R. A. F. Dixon, E. M. Scolnick, I. S. Sigal, *Proc. Natl. Acad. Sci. USA* **1988**, *85*, 4686–4690.
[18] S. Virgil in *Methods and Principles in Medicinal Chemistry, Vol. 45* (Ed.: A. K. Ghosh), Wiley-VCH, Weinheim, **2010**, pp. 139–168.
[19] H. Mitsuya, J. Erickson in *Textbook of AIDS Medicine* (Eds.: T. Merigan, J. Bartlett, D. Bolgnesi), Williams & Wilkis, Baltimore, **1999**, pp. 751–780.
[20] M. Glesby in *Protease Inhibitors in AIDS Therapy*, (Eds.: R. Ogden, C. Flexner), Marcel Dekker, New York, **2001**, pp. 237–256.
[21] A. Wensing, N. M. van Maarseveen, M. Nijhuis, *Antiviral Res.* **2010**, *85*, 59–74.
[22] S. Grabar, C. Pradier, E. Le Corfec, R. Lancar, C. Allavena, M. Bentata, P. Berlureau, C. Dupont, P. Fabbro-Peray, I. Poizot-Martin, D. Costagliola, *AIDS* **2000**, *14*, 141–149.
[23] M. Wainberg, G. Friedland, *JAMA J. Am. Med. Assoc.* **1998**, *279*, 1977–1983.
[24] L. Mansky, H. Temin, *J. Virol.* **1995**, *69*, 5087–5094.
[25] J. Drake, J. Holland, *Proc. Natl. Acad. Sci. USA* **1999**, *96*, 13910–13913.
[26] A. Perelson, A. Neumann, M. Markowitz, J. Leonard, D. Ho, *Science* **1996**, *271*, 1582–1586.
[27] D. Robertson, B. Hahn, P. Sharp, *J. Mol. Evol.* **1995**, *40*, 249–259.
[28] A. Leigh Brown, *Proc. Natl. Acad. Sci. USA* **1997**, *94*, 1862–1865.
[29] R. Steigbigel, D. Cooper, P. Kumar, et al., *N. Engl. J. Med.* **2008**, *359*, 339–354.
[30] J. Stephenson, *J. Am. Med. Assoc.* **2007**, *297*, 1535–1536.
[31] P. Cane, J. Antimicro, *Chemoth* **2009**, *Suppl. 1*, i37–i40.
[32] B. Dau, M. Holodniy, *Drugs* **2009**, *69*, 31–50.
[33] C. Stoddart, P. Joshi, B. Sloan, J. Bare, P. Smith, G. Allaway, C. Wild, D. Martin, *PLoS ONE* **2007**, *2*, e1251.
[34] J. Tazi, N. Bakkour, V. Marchand, L. Ayadi, A. Aboufirassi, C. Branlant, *FEBS J.* **2010**, *277*, 867–876.
[35] H. Mitsuya, A. Ghosh in *Aspartic Acid Proteases as Therapeutic Targets* (Ed.: A. Ghosh), Wiley-VCH, Weinheim, **2010**, pp. 245–262.
[36] E. Domingo, R. Webster, J. Holland in *Origins and Evolution of Viruses*, Academic Press, London, **1999**, pp. 197–224.
[37] A. Ali, R. Bandaranayake, Y. Cai, N. King, M. Kolli, S. Mittal, J. Murzycki, M. Nalam, E. Nalivaika, A. Ozen, M. Prabu-Jeyabalan, K. Thayer, C. Schiffer, *Viruses* **2010**, *2*, 2509–2535.
[38] L. Menéndez-Arias, *Antiviral Res.* **2010**, *85*, 210–231.
[39] A. Wensing, N. Maarseveen, M. Nijhuis, *Antiviral Res.* **2010**, *59–74*.

[40] S. V. Gulnik, L. I. Suvorov, B. Liu, B. Yu, B. Anderson, H. Mitsuya, J. W. Erickson, *Biochemistry* **1995**, *34*, 9282–9287.
[41] R. Kantor, W. J. Fessel, A. R. Zolopa, D. Israelski, N. Shulman, J. G. Montoya, M. Harbour, J. M. Schapiro, R. W. Shafer, *Antimicrob. Agents Chemother.* **2002**, *46*, 1086–1092.
[42] K. Yusa, W. Song, M. Bartelmann, S. Harada, *J. Virol.* **2002**, *76*, 3031–3037.
[43] G. Croteau, L. Doyon, D. Thibeault, G. McKercher, L. Pilote, D. Lamarre, *J. Virol.* **1997**, *71*, 1089–1096.
[44] J. Martinez-Picado, A. V. Savara, L. Sutton, R. T. D'Aquila, *J. Virol.* **1999**, *73*, 3744–3752.
[45] J. Condra, W. Schleif, O. Blahy, L. Gabryelski, D. J. Graham, J. C. Quintero, A. Rhodes, H. L. Robbins, E. Roth, M. Shivaprakash, D. Titus, T. Yang, H. Tepplert, K. E. Squires, P. J. Deutsch, E. A. Emini, *Nature* **1995**, *374*, 569–571.
[46] S. Tamiya, S. Mardy, M. Kavlick, K. Yoshimura, H. Mitsuya, *J. Virol.* **2004**, *78*, 12030–12040.
[47] F. Mammano, C. Petit, F. Clavel, *J. Virol.* **1998**, *72*, 7632–7637.
[48] L. Hong, X. Zhang, J. A. Hartsuck, J. Tang, *Protein Sci.* **2000**, *9*, 1898–1904.
[49] G. S. Laco, C. Schalk-Hihi, J. Lubkowski, G. Morris, A. Zdanov, A. Olson, J. H. Elder, A. Wlodawer, A. Gustchina, *Biochemistry* **1997**, *36*, 10696–10708.
[50] A. K. Ghosh, B. Chapsal, I. Weber, H. Mitsuya, *Acc. Chem. Res.* **2008**, *41*, 78–86.
[51] A. K. Ghosh, P. R. Sridhar, S. Leshchenko, A. K. Hussain, J. Li, A. Y. Kovalevsky, D. E. Walters, J. Wedekind, V. Grum-Tokars, D. Das, Y. Koh, K. Maeda, H. Gatanaga, I. T. Weber, H. Mitsuya, *J. Med. Chem.* **2006**, *49*, 5252–5261.
[52] J. Agniswamy, I. T. Weber, *Viruses* **2009**, *1*, 1110–1136.
[53] A. Wlodawer, J. Vondrasek, *Annu. Rev. Biophys. Biomol. Struct.* **1998**, *27*, 249–284.
[54] C. Chothia, A. Lesk, *Cold Spring Harbor Symp. Quant. Biol.* **1987**, *52*, 399–405.
[55] C. Worth, S. Gong, T. Blundell, *Nat. Rev. Mol. Cell Biol.* **2009**, *10*, 709–720.
[56] A. Todd, C. Orengo, J. Thornton, *Curr. Opin. Chem. Biol.* **1999**, *3*, 548–556.
[57] J. Liang, H. Edelsbrunner, C. Woodward, *Protein Sci.* **1998**, *7*, 1884–1897.
[58] R. Wolfenden, M. J. Snider, *Acc. Chem. Res.* **2001**, *34*, 938–945.
[59] S. J. Benkovic, S. Hammes-Schiffer, *Science* **2003**, *301*, 1196–1202.
[60] M. Garcia-Viloca, J. Gao, M. Karplus, D. G. Truhlar, *Science* **2004**, *303*, 186–195.
[61] A. Wlodawer, M. Miller, M. Jaskolski, B. K. Sathyanarayana, E. Baldwin, I. T. Weber, L. M. Selk, L. Clawson, J. Schneider, S. B. Kent, *Science* **1989**, *245*, 616–621.
[62] A. Gustchina, I. T. Weber, *FEBS Lett.* **1990**, *269*, 269–272.
[63] A. Gustchina, C. Sansom, M. Prevost, J. Richelle, S. Y. Wodak, A. Wlodawer, I. T. Weber, *Protein Eng.* **1994**, *7*, 309–317.
[64] Y. Tie, P. I. Boross, Y. F. Wang, L. Gaddis, F. Liu, X. Chen, J. Tozser, R. W. Harrison, I. T. Weber, *FEBS J.* **2005**, *272*, 5265–5277.
[65] A. Wlodawer, A. Gustchina, *Biochim. Biophys. Acta Protein Struct. Mol. Enzymol.* **2000**, *1477*, 16–34.
[66] W. Wang, P. A. Kollman, *Proc. Natl. Acad. Sci. USA* **2001**, *98*, 14937–14942.
[67] A. K. Ghosh, P. R. Sridhar, N. Kumaragurubaran, Y. Koh, I. T. Weber, H. Mitsuya, *ChemMedChem* **2006**, *1*, 939–950.
[68] A. K. Ghosh, *J. Med. Chem.* **2009**, *52*, 2163–2176.
[69] A. Y. Kovalevsky, F. Liu, S. Leshchenko, A. K. Ghosh, J. M. Louis, R. W. Harrison, I. T. Weber, *J. Mol. Biol.* **2006**, *363*, 161–173.
[70] F. Liu, P. I. Boross, Y. F. Wang, J. Tozser, J. M. Louis, R. W. Harrison, I. T. Weber, *J. Mol. Biol.* **2005**, *354*, 789–800.
[71] A. Y. Kovalevsky, Y. Tie, F. Liu, P. I. Boross, Y. F. Wang, S. Leshchenko, A. K. Ghosh, R. W. Harrison, I. T. Weber, *J. Med. Chem.* **2006**, *49*, 1379–1387.
[72] F. Liu, A. Y. Kovalevsky, J. M. Louis, P. I. Boross, Y. F. Wang, R. W. Harrison, I. T. Weber, *J. Mol. Biol.* **2006**, *358*, 1191–1199.
[73] B. Mahalingam, Y. F. Wang, P. I. Boross, J. Tozser, J. M. Louis, R. W. Harrison, I. T. Weber, *Eur. J. Biochem.* **2004**, *271*, 1516–1524.
[74] Y. Tie, A. Y. Kovalevsky, P. Boross, Y. F. Wang, A. K. Ghosh, J. Tozser, R. W. Harrison, I. T. Weber, *Proteins Struct. Funct. Bioinf.* **2007**, *67*, 232–242.
[75] P. Martin, J. F. Vickrey, G. Proteasa, Y. L. Jimenez, Z. Wawrzak, M. A. Winters, T. C. Merigan, L. C. Kovari, *Structure* **2005**, *13*, 1887–1895.
[76] C. H. Shen, Y. F. Wang, A. Y. Kovalevsky, R. W. Harrison, I. T. Weber, *FEBS J.* **2010**, *277*, 3699–3714.
[77] J. F. Miller, C. W. Andrews, M. Brieger, E. S. Furfine, M. R. Hale, M. H. Hanlon, R. J. Hazen, I. Kaldor, et al., *Bioorg. Med. Chem. Lett.* **2006**, *16*, 1788–1794.
[78] J. C. Clemente, R. E. Moose, R. Hemrajani, L. R. Whitford, L. Govindasamy, R. Reutzel, R. McKenna, M. Agbandje-McKenna, M. M. Goodenow, B. M. Dunn, *Biochemistry* **2004**, *43*, 12141–12151.
[79] Z. Chen, Y. Li, E. Chen, D. L. Hall, P. L. Darke, C. Culberson, J. A. Shafer, L. C. Kuo, *J. Biol. Chem.* **1994**, *269*, 26344–26348.
[80] A. K. Ghosh, S. Gemma, E. Simoni, A. Baldridge, D. E. Waters, K. Ide, Y. Tojo, Y. Koh, H. Mitsuya, *Bioorg. Med. Chem. Lett.* **2010**, *20*, 1241–1246.
[81] A. K. Ghosh, J. F. Kincaid, W. Cho, D. E. Walters, K. Krishnan, K. A. Hussain, Y. Koo, H. Cho, C. Rudall, L. Holland, J. Buthod, *Bioorg. Med. Chem. Lett.* **1998**, *8*, 687–690.
[82] K. Yoshimura, R. Kato, M. F. Kavlck, A. Nguyen, V. Maroun, K. Maeda, K. A. Hussain, A. K. Ghosh, S. V. Gulnik, J. W. Erickson, H. Mistuya, *J. Virol.* **2002**, *76*, 1349–1358.
[83] A. K. Ghosh, Z. L. Dawson, H. Mitsuya, *Bioorg. Med. Chem.* **2007**, *15*, 7576–7580.
[84] A. K. Ghosh, B. D. Chapsal, H. Mitsuaya in *Aspartic Acid Proteases as Therapeutic Targets* (Ed.: A. K. Ghosh), Wiley-VCH, Weinheim, **2010**, pp. 205–235.
[85] N. A. Roberts, J. A. Martin, D. Kinchington, A. V. Broadhurst, J. C. Craig, I. B. Duncan, S. A. Galpin, B. K. Handa, J. Kay, A. Krohn, R. W. Lambert, J. H. Merrett, J. S. Mills, K. E. B. Parkes, S. Redshaw, A. J. Ritchie, D. L. Taylor, G. J. Thomas, P. J. Machin, *Science* **1990**, *248*, 358–361.
[86] A. Krohn, S. Redshaw, J. C. Ritchie, B. J. Graves, M. H. Hatada, *J. Med. Chem.* **1991**, *34*, 3340–3342.
[87] K. Nakanishi, *Bioorg. Med. Chem.* **2005**, *13*, 4987–5000.
[88] A. L. Donoho, *J. Anim. Sci.* **1984**, *58*, 1528–1539.
[89] A. K. Ghosh, W. J. Thompson, M. K. Holloway, S. P. McKee, T. T. Duong, H. Y. Lee, P. M. Munson, A. M. Smith, J. M. Wai, P. L. Darke, et al., *J. Med. Chem.* **1993**, *36*, 2300–2310.
[90] A. K. Ghosh, W. J. Thompson, S. P. McKee, T. T. Duong, T. A. Lyle, J. C. Chen, P. L. Darke, J. A. Zugay, E. A. Emini, W. A. Schleif, et al., *J. Med. Chem.* **1993**, *36*, 292–294.
[91] M. L. Vazquez, M. L. Bryant, M. Clare, G. A. DeCrescenzo, E. M. Doherty, J. N. Freskos, D. P. Getman, K. A. Houseman, J. A. Julien, G. P. Kocan, *J. Med. Chem.* **1995**, *38*, 581–584.
[92] R. D. Tung, D. J. Livingston, B. G. Rao, E. E. Kim, C. T. Baker, J. S. Boger, S. P. Chambers, D. D. Deininger, M. Dwyer, L. Elsayed, J. Fulghum, B. Li, M. A. Murcko, M. A. Navia, P. Novak, S. Pazhanisamy, C. Stuver, J. A. Thomson in *Protease Inhibitors in AIDS* Therapy (Eds.: R. C. Ogden, C. W. Flexner), Marcel Dekker, New York, **2001**, pp. 101–137.
[93] E. E. Kim, C. T. Baker, M. D. Dwyer, M. A. Murcko, B. G. Rao, R. D. Tung, M. A. Navia, *J. Am. Chem. Soc.* **1995**, *117*, 1181–1182.

[94] A. K. Ghosh, J. F. Kincaid, D. E. Walters, Y. Chen, N. C. Chaudhuri, W. J. Thompson, C. Culberson, P. M. Fitzgerald, H. Y. Lee, S. P. McKee, P. M. Munson, T. T. Duong, P. L. Darke, J. A. Zugay, W. A. Schleif, M. G. Axel, J. Lin, J. R. Huff, *J. Med. Chem.* **1996**, *39*, 3278–3290.

[95] A. K. Ghosh, S. Kulkarni, D. D. Anderson, L. Hong, A. Baldridge, Y.-F. Wang, A. A. Chumanevich, A. Y. Kovalevsky, Y. Tojo, M. Amano, Y. Koh, J. Tang, I. T. Weber, H. Mitsuya, *J. Med. Chem.* **2009**, *52*, 7689–7705.

[96] J. W. Erickson, S. V. Gulnik, H. Mitsuya, A. K. Ghosh (Fitness Assay and Associated Methods), US Patent 7470506B1, **2008**.

[97] S. De Meyer, M. Peters, Abstracts 533 and 620, *11th Conference on Retroviruses and Opportunistic Infections (CROI)*, February 8–11 **2004**, San Francisco, CA (USA).

[98] R. Hoetelmans, I. van der Sandt, M. De Pauw, K. Struble, M. Peeters, R. van der Geest, Abstract 549, *10th Conference on Retroviruses and Opportunistic Infections (CROI)*, February **2003**, Boston, MA (USA).

[99] D. L. Surleraux, A. Tahri, W. G. Verschueren, G. M. Pille, H. A. De Kock, T. H. Jonckers, A. Peeters, S. De Meyer, H. Azjin, R. Pauwels, M. P. de Bethune, N. M. King, M. Prabu-Jeyabalan, C. A. Schiffer, P. B. Wigerinck, *J. Med. Chem.* **2005**, *48*, 1813–1822.

[100] Y. Tie, P. Boross, Y. Wang, L. Gaddis, A. Hussain, S. Leshchenko, A. Ghosh, J. Louis, R. Harrison, I. Weber, *J. Mol. Biol.* **2004**, *338*, 341–352.

[101] N. King, M. Prabu-Jeyabalan, E. Nalivaika, P. Wigerinck, M. de Bethune, C. Schiffer, *J. Virol.* **2004**, *78*, 12012–12021.

[102] I. Dierynck, I. Keuleers, M. De Wit, A. Tahri, D. Surleraux, D. A. Peeters, K. Hertogs, *Antiviral Res.* **2005**, *10*, S71.

[103] E. Lefebvre, C. Schiffer, *AIDS Rev.* **2008**, *10*, 131–142.

[104] A. Kovalevsky, A. K. Ghosh, I. T. Weber, *J. Med. Chem.* **2008**, *51*, 6599–6603.

[105] Y. Koh, H. Nakata, K. Maeda, H. Ogata, H. G. Bilcer, T. Devasamudram, J. F. Kincaid, P. Boross, Y. F. Wang, Y. Tie, P. Volarath, L. Gaddis, R. W. Harrison, I. T. Weber, A. K. Ghosh, H. Mitsuya, *Antimicrob. Agents Chemother.* **2003**, *47*, 3123–3129.

[106] S. De Meyer, H. Azijn, D. Surleraux, D. Jochmans, A. Tahri, R. Pauwels, P. Wigerinck, M. de Bethune, *Antimicrob. Agents Chemother.* **2005**, *49*, 2314–2321.

[107] Y. Koh, M. Amano, T. Towata, M. Danish, S. Leshchenko-Yashchuk, D. Das, M. Nakayama, Y. Tojo, A. K. Ghosh, H. Mitsuya, *J. Virol.* **2010**, *84*, 11961–11969.

[108] S. De Meyer, A. Hill, I. De Baere, I. Rimsky, H. Azijin, B. Van Baelen, E. De Paepe, T. Vangeneugden, et al., *Antiviral Ther.* **2006**, *11*, S73.

[109] C. Wolfe, C. Hicks, *HIV/AIDS* **2009**, *1*, 13–21.

[110] K. Saskova, M. Kozisek, P. Rezacova, J. Brynda, T. Yashina, R. Kagan, J. Konvalinka, *J. Virol.* **2009**, *83*, 8810–8818.

[111] A. Wlodwaer, M. Miller, M. Jaskolski, B. Sathyanarayana, E. Baldwin, I. Weber, L. Selk, L. Clawson, *Science* **1989**, *245*, 616–621.

[112] Y. Koh, S. Matsumi, D. Das, M. Amano, D. Davis, J. Li, S. Leschenko, A. Baldridge, et al., *J. Biol. Chem.* **2007**, *282*, 28709–28720.

[113] M. Amano, Y. Koh, D. Das, J. Li, S. Leschenko, Y. F. Wang, P. I. Boross, I. T. Weber, A. K. Ghosh, H. Mitsuya, *Antimicrob. Agents Chemother.* **2007**, *51*, 2143–2155.

[114] Y. F. Wang, Y. Tie, P. I. Boross, J. Tozser, A. K. Ghosh, R. W. Harrison, I. T. Weber, *J. Med. Chem.* **2007**, *50*, 4509–4515.

[115] J. F. Miller, E. S. Furfine, M. H. Hanlon, R. J. Hazen, J. A. Ray, L. Robinson, V. Samano, A. Spaltenstein, *Bioorg. Med. Chem. Lett.* **2004**, *14*, 959–963.

[116] R. Hazen, R. Harvey, R. Ferris, C. Craig, P. Yates, P. Griffin, J. Miller, I. Kaldor, J. Ray, V. Samano, E. Furfine, A. Spaltenstein, M. Hale, R. Tung, M. St. Clair, M. Hanlon, L. Boone, *Antimicrob. Agents Chemother.* **2007**, *51*, 3147–3154.

[117] S. L. Ford, Y. S. Reddy, M. T. Anderson, S. C. Murray, P. Fernandez, D. S. Stein, M. A. Johnson, *Antimicrob. Agents Chemother.* **2006**, *50*, 2201–2206.

[118] J. R. Lalezari, D. J. Ward, S. A. Tomkin, H. R. Garges, *J. Antimicrob. Chemother.* **2007**, *60*, 170–174.

[119] Corresponding press release online: "GlaxoSmithKline Discontinues Clinical Development of Investigational Protease Inhibitor Brecanavir (640385)". http://www.gsk.com/media/pressreleases/2006/2006_12_18_GSK945.htm.

[120] A. K. Ghosh, J. Li, H. Mitsuya, unpublished work, Purdue University and National Cancer Institute.

[121] T. Cihlar, G. X. He, X. Liu, J. M. Chen, M. Hatada, S. Swaminathan, M. J. McDermott, Z. Y. Yang, et al., *J. Mol. Biol.* **2006**, *363*, 635–647.

[122] C. Callebaut, K. Stray, L. Tsai, L. H. Xu, G. X. He, A. Mulato, T. Priskich, N. Parkin, et al., *20th International Conference on Antiviral Research*; Palm Spring, CA, April 29 to May 3, **2007**, p. 2.

[123] C. Callebaut, K. Stray, L. Tsai, M. Williams, Z. Yang, C. Cannizzaro, S. A. Leavitt, X. Liu, K. Wang, B. P. Murray, A. Mulato, M. Hatada, T. Priskich, N. Parkin, S. Swaminathan, W. Lee, G. He, L. Xu, T. Cihlar, *Antimicrob. Agents Chemother.* **2011**, *55*, 1366–1376.

[124] A. Gustchina, I. T. Weber, *FEBS Lett.* **1990**, *269*, 269–272.

[125] A. K. Ghosh, C. D. Martyr, M. Steffey, Y.-F. Wang, J. Agniswamy, M. Amano, I. T. Weber, H. Mitsuya, *ACS Med. Chem. Lett.* **2011**, *2*, 298–302.

[126] D. J. Kempf, K. C. Marsh, D. A. Paul, M. F. Knige, D. W. Norbeck, W. E. Kohlbrenner, L. Codacovi, S. Vasavanonda, P. Bryant, X. C. Wang, N. E. Wideburg, J. J. Clement, J. J. Plattner, J. Erickson, *Antimicrob. Agents Chemother.* **1991**, *35*, 2209–2214.

[127] E. T. Baldwin, T. N. Bhat, B. Liu, N. Pattabriaman, J. W. Erickson, *Struct. Biol.* **1995**, *2*, 244–249.

[128] Y. Tojo, Y. Koh, M. Amano, M. Aoki, D. Das, A. K. Ghosh, H. Mitsuya, *Antimicrob. Agents Chemother.* **2010**, *54*, 3460–3470.

[129] A. K. Ghosh, S. Gemma, J. Takayama, A. Baldridge, S. Leshchenko-Yashchuk, H. B. Miller, Y.-F. Wang, A. Y. Kovalevsky, Y. Koh, I. T. Weber, H. Mitsuya, *Org. Biomol. Chem.* **2008**, *6*, 3703–3713.

[130] A. K. Ghosh, B. Chapsal, G. L. Parham, M. P. Steffey, J. Agniswamy, Y.-F. Wang, M. Amano, I. T. Weber, H. Mitsuya, *J. Med. Chem.* **2011**, *54*, 5890–5901.

[131] A. K. Ghosh, S. Leshchenko-Yashchuk, D. D. Anderson, A. Baldridge, M. Noetzel, H. B. Miller, Y. Tie, Y.-F. Wang, Y. Koh, I. T. Weber, H. Mitsuya, *J. Med. Chem.* **2009**, *52*, 3902–3914.

[132] Y. Koh, D. Das, S. Leshchenko, H. Nakata, H. Ogata-Aoki, M. Amano, M. Nakayama, A. K. Ghosh, H. Mitsuya, *Antimicrob. Agents Chemother.* **2009**, *53*, 997–1006.

[133] A. K. Ghosh, S. Gemma, A. Baldridge, Y. F. Wang, A. Y. Kovalevsky, Y. Koh, I. T. Weber, H. Mitsuya, *J. Med. Chem.* **2008**, *51*, 6021–6033.

[134] A. K. Ghosh, B. Chapsal, A. Baldridge, M. P. Steffey, D. E. Walters, Y. Koh, M. Amano, H. Mitsuya, *J. Med. Chem.* **2011**, *54*, 622–634.

[135] K. Ide, M. Aoki, M. Amano, Y. Koh, R. S. Yedidi, D. Das, S. Leschenko, B. Chapsal, A. K. Ghosh, H. Mitsuya, *Antimicrob. Agents Chemother.* **2011**, *55*, 1717–1727.

[136] T. A. Halgren, *J. Comput. Chem.* **1999**, *20*, 730–748.

[137] A. K. Ghosh, C. X. Xu, K. V. Rao, A. Baldridge, J. Agniswamy, Y. F. Wang, I. T. Weber, M. Aoki, S. G. P. Miguel, M. Amano, H. Mitsuya, *ChemMedChem* **2010**, *5*, 1850–1854.

AAC
Journals.ASM.org

Mechanism of Interaction of Human Mitochondrial DNA Polymerase γ with the Novel Nucleoside Reverse Transcriptase Inhibitor 4′-Ethynyl-2-Fluoro-2′-Deoxyadenosine Indicates a Low Potential for Host Toxicity

Christal D. Sohl,[a] Kamlendra Singh,[b] Rajesh Kasiviswanathan,[c] William C. Copeland,[c] Hiroaki Mitsuya,[d,e] Stefan G. Sarafianos,[b] and Karen S. Anderson[a]

Department of Pharmacology, Yale University School of Medicine, New Haven, Connecticut, USA[a]; Department of Molecular Microbiology and Immunology, University of Missouri School of Medicine, Columbia, Missouri, USA[b]; Laboratory of Molecular Genetics, National Institute of Environmental Health Sciences, National Institutes of Health, DHHS, Research Triangle Park, North Carolina, USA[c]; Departments of Infectious Diseases and Hematology, Kumamoto University Graduate School of Medical Sciences, Kumamoto, Japan[d]; and Experimental Retrovirology Section, HIV and AIDS Malignancy Branch, National Cancer Institute, National Institutes of Health, Bethesda, Maryland, USA[e]

The potent antiretroviral 4′-ethynyl-2-fluoro-2′-deoxyadenosine (EFdA) is a promising experimental agent for treating HIV infection. Pre-steady-state kinetics were used to characterize the interaction of EFdA-triphosphate (EFdA-TP) with human mitochondrial DNA polymerase γ (Pol γ) to assess the potential for toxicity. Pol γ incorporated EFdA-TP 4,300-fold less efficiently than dATP, with an excision rate similar to ddATP. This strongly indicates EFdA is a poor Pol γ substrate, suggesting minimal Pol γ-mediated toxicity, although this should be examined under clinical settings.

Nucleoside reverse transcriptase inhibitors (NRTIs) are a critical component of highly active antiretroviral therapy for treating HIV infection. All FDA-approved NRTIs are nucleoside analogs lacking a 3′-hydroxyl group, forcing DNA chain termination upon incorporation by viral reverse transcriptase (RT). A central source of toxicity stems from the interaction of NRTIs with human mitochondrial DNA polymerase γ (Pol γ), the only human polymerase capable of using these drugs as substrates (2, 16, 18, 20). Incorporation of NRTIs can result in chain termination during replication, causing mitochondrial DNA depletion that can manifest in patients as myopathies, lipodystrophies, lactic acidosis, or liver failure (2–4, 12).

Current NRTIs can be plagued with toxicity and RT resistance, so there is a critical need for new antivirals. A promising new NRTI is 4′-ethynyl-2-fluoro-2′-deoxyadenosine (EFdA) (Fig. 1A) (17). Its 50% effective concentration (EC_{50}) of 50 pM is one of the best reported for an NRTI, 440-fold better than zidovudine (AZT) and 66,000-fold better than tenofovir, and numerous NRTI-resistant strains of HIV also show sensitivity and even hypersensitivity to EFdA (13, 17, 24, 27). It is also effective *in vivo*, causing a significant decrease in viral load and low toxicity in a humanized HIV-infected mouse model (9).

Despite the 3′-hydroxyl group, EFdA acts as a chain terminator by preventing RT translocation (24). This is in contrast to KP-1212, another 3′-hydroxyl-containing NRTI that facilitates error-prone extension by RT (1, 25). The 4′-ethynyl group locks the sugar in a favorable position for incorporation, which, along with the 3′-hydroxyl, makes EFdA a better substrate for RT than native nucleotides (15, 24). Similarly, EFdA may be preferred by Pol γ, but kinetic studies are limited to a 50% inhibitory concentration (IC_{50}) of 10 μM and a K_i of 25 μM for Pol γ (26, 27), indicating that EFdA serves as a substrate. In this study, we sought to expand our prior work with EFdA (26) to characterize the molecular mechanism of inhibition of Pol γ by EFdA. Such studies are critical to assess the safety of drugs in preclinical and clinical trials.

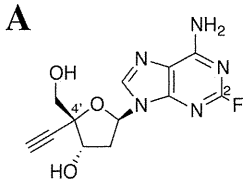

FIG 1 (A) Structure of EFdA. (B) DNA oligonucleotides used in the experiments. Shown are the D21 primer (radiolabeled, as indicated by an asterisk) and the D36 template. The primer "X" is the site of incorporation of the incoming dATP or EFdA-TP used in the single-nucleotide incorporation experiments or the location of the EFdA-MP to be removed in the excision studies.

Assessing the potential for Pol γ-mediated toxicity requires discerning the individual rate constants of NRTI incorporation and excision using pre-steady-state kinetics. Since steady-state studies report only on the rate-limiting step, which for Pol γ is product release, pre-steady-state kinetics are required to determine NRTI affinity and rates of NRTI incorporation and excision by Pol γ, which provides a detailed kinetic mechanism of *in vitro* toxicity. Single-turnover conditions, in which the enzyme is in excess of the substrate, were used to generate k_{pol}, the maximum rate of polymerization, and K_d, the binding affinity for the incom-

Received 14 September 2011 Returned for modification 7 November 2011
Accepted 2 December 2011
Published ahead of print 12 December 2011
Address correspondence to Karen S. Anderson, karen.anderson@yale.edu.

doi:10.1128/AAC.05729-11